INFLUENCE OF TIG PROCESS PARAMETERS ON HARDNESS, TENSILE STRENGTH AND MICROSTRUCTURES OF AISI430 FERRITIC STAINLESS STEEL WELDS

BY

ABDULRAHMAN ADEIZA MUSA

DEPARTMENT OF METALLURGICAL AND MATERIALS ENGINEERING,
AHMADU BELLO UNIVERSITY,
ZARIA, NIGERIA

MARCH, 2021

INFLUENCE OF TIG PROCESS PARAMETERS ON HARDNESS, TENSILE STRENGTH AND MICROSTRUCTURES OF AISI430 FERRITIC STAINLESS STEEL WELDS

BY

Abdulrahman Adeiza MUSA,
B.Eng. (Met. & Mats.) 2015
(P17EGML8001)

A THESIS SUBMITTED TO THE SCHOOL OF POSTGRADUATE STUDIES
AHMADU BELLO UNIVERSITY, ZARIA NIGERIA,
IN PARTIAL FULFILLMENT OF THE REQUIREMENTS FOR THE AWARD OF MASTER OF SCIENCE IN METALLURGICAL AND MATERIALS ENGINEERING

DEPARTMENT OF METALLURGICAL AND MATERIALS ENGINEERING,
FACULTY OF ENGINEERING,
AHMADU BELLO UNIVERSITY,
ZARIA - NIGERIA

MARCH, 2021

DECLARATION

I declare that the work in thisdissertationentitled "Influence of TIGProcess Parameters on Hardness, Tensile Strength and Microstructuresof AISI430 Ferritic Stainless Steel Welds”has been performed by me in the Department of Metallurgical and Materials Engineering. The information derived from the literature has been duly acknowledged in the text and a list of references provided. No part of this dissertation was previously presented for another degree or diploma at this or any other Institution.

Musa, Abdulrahman Adeiza _____ _____
SignatureDate

CERTIFICATION

This dissertation entitled INFLUENCE OFTIG PROCESS PARAMETERS ON HARDNESS, TENSILE STRENGTH AND MICROSTRUCTURES OF AISI430 FERRITIC STAINLESS STEEL WELDS by Abdulrahman AdeizaMUSA meets the regulations governing the award of the Degree of Masters of Science in Metallurgical and Materials Engineering, Ahmadu Bello University Zaria, and is approved for its contribution to knowledge and literary presentation.

Prof. E.T. Dauda _____ _____

Chairman, Supervisory CommitteeSignatureDate

Dr. K.A. Bello _____ _____

Member, Supervisory CommitteeSignatureDate

Prof. R. A. Mohammed _____ _____

Head of DepartmentSignatureDate

Prof. Sani A. Abdullahi _____ _____

Dean, School of Postgraduate Studies Signature Date

ACKNOWLEDGEMENT

All praises and thanks are to Almighty ALLAH Who has made the completion of this work successful. First, I will like to extend my special thanks to my beloved mother MallamaHabibatMayaki, my elder sister, Musa MemunatEneze and all my brothers for their spiritual and moral support. I also owe special thanks to my beloved wife, Hassan LauratuOyizawho has always stood beside me in prayers to make sure this work sees the light of the day, thank you so much dear, may Almighty Allah keep us together, Ameen.

My profound gratitude goes to my supervisors, Prof. E.T Dauda and Dr. K.A Bello for their endless support and words of encouragement during the course of my research work.They were never tired of listening and proffering solutions to my problems; I appreciate you all sir.

I also appreciate all our technical staff in the Department of the Metallurgical and Materials Engineering particularly Mal. Suleiman and Oga Tunde for their insightful contribution towards the completion of this work. I won't forget Mal. Abdul Rasheed who has assisted me in performing some of the experiments at the Department of Metallurgical and Materials Engineering, A.B.U Zaria. May God Almighty bless you all.

I will also like to express my appreciation to the Head of DepartmentProf. R.A Mohammed, the formal Head of Department Dr.Auwal Kasim,Departmental PG coordinator, Dr. Umar Shehu and the entire staffof the Department of Metallurgical and Materials Engineering, Ahmadu Bello University, Zariafor their kind hearted support and encouragement. May Almighty Allah reward you all. I also appreciate my friends and all my class mates, who have contributed in one way or the other towards the success of this research work.

Above all, I thank the Almighty God, the Beginning and the End for His love and mercies upon our lives.

ABSTRACT

The influence of tungsten inert gas (TIG) welding process parameters on the microstructural features and mechanical properties (hardness and tensile strength) of AISI430 ferritic stainless steel (FSS) weldsbased on the central composite design (CCD) approach, was investigated. The process parameters considered in this study include; the welding current (I), welding speed (S) and argon flow rate (AFR). The stainless steel AISI 430 FSS plates having chromium content of 17% Cr and 1.5mm thickness were butt-welded using autogenous tungsten inert gas welding process. The microstructures of the FSS welds were analyzed using optical microscope.The hardness and tensile strength were determined using Vickers's microhardness testing machine and Hounsfield tensile testing machine respectively. The results showed that all input variables considered have direct influence on the properties as well as the microstructure of the weldments. Microstructural result reveals ferrite structures aligned in the cold rolling direction for the base metal. The microstructure of the weld metal at the optimized conditionshows the presence of equiaxed ferrite grains with some grain boundary martensitestructureswithin the fusion and heat affected zones of theweldment. It was observed that welding current shows the greatest effect on the tensile strengthwith34% contribution, followed by the speed and argon flow rate with 15% and 2.54% respectively. For the hardness, the speed plays the major role. Empirical models were generated from the analysis to predict the weld quality. An optimized tensile strength and hardness of 431.014MPa and 307.10 HV respectively, were predicted at the welding current of 22A, the welding speed of 5mm/s and the argon flow rate of 10L/min. In order to validate the results, confirmatory experiments were performed based at the optimized condition and the test results were found to be in good agreement with the predicted values with percentage errors of 1.23% and 1.81% for the tensile strength and hardness respectively. Based on this finding, it can be concluded that the optimization of TIG input parameters usingresponse surface

methodologyapproach produced weld joint with good tensile strength and improved hardness that is very close to that of the base metal.

Table of Contents

Title Page - - - - - - - - - - - i

Declaration - - - - - - - - - - - ii

Certification - - - - - - - - - - - iii

Acknowledgement - - - - - - - - - - iv

Abstract - - - - - - - - - - - v

Table of contents - - - - - - - - - - vi

List of Tables - - - - - - - - - - x

List of Figures - - - - - - - - - - xi

List of Plates - - - - - - - - - - xiii

Abbreviations - - - - - - - - - - xiv

CHAPTER ONE

INTRODUCTION - - - - - - - - - - 1

1.1 Background of Study - - - - - - - - 3

1.2 Statement of Research Problem - - - - - - - 3

1.3 Aim and Objectives - - - - - - - - - 4

1.4 Scope of the Study - - - - - - - - - 5

1.5 Justification of the Study - - - - - - - - 5

CHAPTER TWO

LITERATURE REVIEW - - - - - - - - -6

2.1 Steels - - - - - - - - - - -6

2.2 Classification of Steels - - - - - - - - -

6

2.2.1 Plain carbon steels - - - - - - - - - 6

2.2.2 Carbon steels - - - - - - - - - - 6

2.2.2*a* Low carbon steel - - - - - - - - -6

2.2.2*b* Medium carbon steel - - - - - - - - -6

2.2.2*c* High carbon steel - - - - - - - - -7

2.2.2*d* Very high carbon steel - - - - - - - -7

2.3 Low-Alloy Steels - - - - - - - - -7

2.4 Stainless Steels - - - - - - - - -7

2.4.1 Austenitic stainless steel - - - - - - - -9

2.4.2 Martensitic stainless steel - - - - - - - -

10

2.4.3 Ferriticstainless steel - - - - - - - - -10

2.4.3.1 Application of ferritic stainless steel - - - - - - -

11

2.5 Microstructure of Steels - - - - - - - - 11

2.6 Fusion Welding - - - - - - - - -12

2.6.1 Shielded metal arc weldingprocess - - - - - - - 13

2.6.2 Gas-metal arc weldingprocess - - - - - - - 14

2.6.3 Tungsten inert gasweldingprocess - - - - - - -

15

2.6.3*a* Process parameters in TIG welding - - - - - - -

16

2.6.3*b* Welding current - - - - - - - - - 16

2.6.3*c* Welding speed- - - - - - - - - - 17

2.7 Welding of Stainless Steels - - - - - - - - 17

2.7.1 Welding of austenitic stainless steels - - - - - - - - 18

2.7.2 Welding of martensitic stainless steels - - - - - - - 19

2.7.3 Welding of ferritic stainless steels - - - - - - - - 20

2.7.3*a* Grain Growth and martensite formation in ferritic stainless steels - - - 20

2.7.3*b* Problems with ferritic stainless steel weld - - - - - - 22

2.8 Design of Experiment Techniques - - - - - - - 23

2.8.1 Factorial design - - - - - - - - - 23

2.8.2 Response surface methodology - - - - - - - 24

2.8.2*a* Central composite design - - - - - - - - - 25

2.8.2*b* Box-Behnken design - - - - - - - - - 25

2.9 Central Composite Design Optimization Tools - - - - 25

2.9.1 Analysis of Variance (ANOVA) - - - - - - - - 26

2.9.2 Fit summary Statistics - - - - - - - - 26

2.9.3 Box-Cox Transform - - - - - - - - - 26

2.10 Summary of Major Findings on Stainless Steel Welds - - - 26

CHAPTER THREE

MATERIALS AND METHOD - - - - - - - -30

3.1 Introduction - - - - - - - - - -30

3.2 Materials - - - - - - - - - - 30

3.2.1 Equipment - - - - - - - - - -31

3.3 Methodology - - - - - - - - - -31

3.3.1 Selection of input factors - - - - - - - - 32

3.3.2 Response variable for the study - - - - - - - 33

3.3.3 Multi-Objective Optimization Process - - - - - - 33

3.3.4 Experimental design matrix - - - - - - - - 34

3.4 TIG Torch Welding Technique - - - - - - - 35

3.5 Material Testing - - - - - - - - -36

3.5.1 Tensile test - - - - - - - - - - 36

3.5.2 Hardness test - - - - - - - - - - 37

3.6 Microstructural Analysis - - - - - - - - 38

CHAPTER FOUR

RESULTS AND DISCUSSION - - - - - - - -40

4.1 Modeling for Tensile Strength - - - - - - - 41

4.1.1 Fit summary statistics for the tensile strength- - - - - -41

4.1.2 Analysis of variance (ANOVA) test results for the tensile strength - - - 41

4.1.3 Model adequacy test and validation for tensile strength - - - - 43

4.1.4 Surface and contour plot for tensile strength - - - - - - 45

4.1.5 Discussion - - - - - - - - - - 49

4.2 Modeling for Hardness - - - - - - - -50

4.2.1 Fit summary statistics for the hardness - - - - - - 50

4.2.2 Analysis of variance (ANOVA) test results forhardness - - - - 51

4.2.3 Model adequacy test and validation for hardness - - - - - 52

4.2.4 Surface and contour plot for hardness - - - - - - 55

4.2.5 Discussion - - - - - - - - - -59

4.3 Multi-Objective Optimization (*MOO*) for Response Performance - -60

4.3.1 Confirmatory test - - - - - - - - -61

4.4 Characteristics of optimized TIG Ferritic Stainless Steel Weld - - -62

4.4.1 Weld topography - - - - - - - - -62

4.4.2 Microstructural analysis - - - - - - - -63

4.4.3 Analysis of the micro-hardness - - - - - - - 67

4.4.4 Analysis of the tensile strength - - - - - - - 69

4.5 Summary - - - - - - - - - - 70

CHAPTER FIVE

CONCLUSION AND RECOMMENDATIONS - - - - - -72

5.1 Conclusion - - - - - - - - - - 72

5.2 Recommendations - - - - - - - - - 73

5.3 Contribution to Knowledge - - - - - - - - 73

REFERENCES - - - - - - - - - -74

APPENDIX - - - - - - - - - - - 80

List of Tables

Table 2.1: Classifications of common-grade wrought stainless steels - - - 8

Table 2.2: Typical physical properties of common grades of stainless steels in comparison with carbon steel - - - - - - - - - 9

Table 3.1: Chemical composition of AISI 430 ferritic stainless steel - - -

30

Table 3.2: Equipment and the Laboratory - - - - - - -

31

Table 3.3: Factors and levels for the CCD experimental design plan- - -33

Table 3.4: Design matrix of process parameters for TIG welding process - - -34

Table 4.1: Design matrix and responses for TIG welding process - - - -

40

Table 4.2: Fit Summary statistics for Tensile strength - - - - -41

Table 4.3: Analysis of variance (ANOVA Table) for the tensile strength - - -42

Table 4.4: Summary of model statistics for Tensile Strength - - - - 45

Table 4.5: Fit Summary statistics for Hardness - - - - - -51

Table 4.6: Analysis of variance (ANOVA Table) for Hardness - - - -52

Table 4.7: Summary of model statistics for Hardness - - - - - 54

Table 4.8: Optimization condition for the process parameter and responses - - 61

Table 4.9: Optimal solution for the responses - - - - - - 61

Table 4.10: Confirmatory test result - - - - - - - -62

Table 4.11: Mechanical properties of base metal and welded metal with optimized parameters - - - - - - - - -62

List of Figures

Figure 2.1:Some microstructures of Steel (a) austenite structure(b) ferrite structure (c) pearlite structure(d) martensite structure - - - - - - -12

Figure 2.2: Basic arc welding circuit diagram - - - - - - 13

Figure 2.3: Shielded metal arc welding process - - - - - -14

Figure 2.4: Gas-Metal Arc Welding Process - - - - - - - -15

Figure 2.5: Gas-Tungsten Arc Welding Process - - - - - - - -16

Figure 2.6: Three different current polarities in TIG Welding - - - - 17

Figure 2.7: Thermal affected areas of metal due to welding - - - - - 18

Figure 2.8: Microstructure of AISI 430 stainless steel (magnification 212X): (*a*) near fusion boundary (*b*) near base metal (*c*) base metal - - - - -21

Figure 2.9: Vertical section of Fe–Cr–C phase diagram (a)showing wt.% Cr at 0.01%C (b) showing the influence of C and N on the gamma-loop. Castro and De Cadenet (1974) - - - - - - - - - - 23

Figure 3.1: Experimental flow chart - - - - - - - - -32

Figure 3.2: TIG welding machine set-up - - - - - - - -35

Figure 3.3: Specimensfor tensile test - - - - - - - -36

Figure 3.4: Vickers microhardness testing machine - - - - - - - 38

Figure 4.1: Perturbation plot for Tensile Strength - - - - - - -43

Figure 4.2: Normal probability plot of residuals for tensile strength - - - 43

Figure 4.3: Plot of residual against predicted values for Tensile strength - - -44

Figure 4.4: Plot of residual versus experimental run order for Tensile strength - -44

Figure 4.5: Box-Cox plot for Tensile strength - - - - - - -44

Figure 4.6: Surface and contour plot showing the variation of Tensile strength with welding current and gas flow rate (a) 3-D surface plot (b) Contour plot - - -46

Figure 4.7: Surface and contour plot showing the variation of Tensile strength with welding currentand welding speed (a) 3-D surface plot (b) Contour plot - -47

Figure 4.8: Surface and contour plot showing the variation of Tensile strength with welding speed and the argon flow rate (a) 3-D surface plot (b) Contour plot - - 48

Figure 4.9: Perturbation plot for Hardness - - - - - - -53

Figure 4.10: Normal probability plot of residuals for the Hardness - - - -53

Figure 4.11: Plot of residual against predicted values for Hardness - - - -53

Figure 4.12: Plot of residual versus experimental run order for Hardness - - - 54

Figure 4.13: Box-Cox plot for Hardness - - - - - - - 54

Figure 4.14: Surface and contour plot showing the variation of Hardness with welding current and speed (a) 3-D surface plot (b) Contour plot - - -56

Figure 4.15: Surface and contour plot showing the variation of Hardness with welding current andthe argon flow rate (a) 3-D surface plot (b) Contour plot - -57

Figure 4.16: Surface and contour plot showing the variation of Hardness with welding speed and the argon flow rate (a) 3-D surface plot (b) Contour plot - - - 58

Figure 4.17: Longitudinal hardness profile across the weld section under different weld conditions - - - - - - - - - 68

Figure 4.18: Influence of welding current on the micro-hardness of the weld - -69

Figure 4.19: Influence of welding speed on the micro-hardness of the weld - - 69

Figure 4.20: Influence of welding current on the tensile strength of theweld - - 70

Figure 4.21: Influence of welding speed on the tensile strength of theweld - -70

List of Plates

Plate 4.1: Topographies of the welds at different heat energy conditions: (a) 58J/mm (b) 174 J/mm (c) 102 J/mm - - - - - - - - -63

Plate 4.2: Micrograph of the base metal etched with 50% Acetic-Nital (x100) - -64

Plate 4.3: Micrograph of TIG welded ferritic stainless steel at 58J/mm (Run 9), etched with 50% Acetic-Nital (x100) - - - - - - - - 64

Plate 4.4: Micrograph of TIG welded ferritic stainless steel at 116J/mm (Run 16), etched with 50% Acetic-Nital (x100) - - - - - - - - 64

Plate 4.5: Micrograph of TIG welded ferritic stainless steel at 116J/mm (Run 16), etched with 50% Acetic-Nital (x100) - - - - - - - - 65

Plate 4.6: Micrograph of TIG welded ferritic stainless steel at 174J/mm (Run 14), etched with 50% Acetic-Nital (x100) - - - - - - - - -65

Plate 4.7: Micrograph of TIG welded ferritic stainless steel at optimizedwelding conditions (102J/mm), etched with 50% Acetic-Nital (x100) - - - - - -65

Abbreviations

%	-	Per cent
A	-	Ampere
AC	-	Alternating current
AFR	-	Argon flow rate
AISI	-	American iron and steel institute
ANOVA	-	Analysis of variance
ASTM	-	American society for testing and materials
BBD	-	Box-Behnken design
BCC	-	Body-centred cubic
C	-	Carbon
CCC	-	Circumscribed central composite
CCD	-	Central composite design
CE	-	Carbon equivalence
Cr	-	Chromium
DC	-	Direct current
DCEN	-	Direct current electrode negative
DCEP	-	Direct current electrode positive
FCAW	-	Flux-cored arc welding
Fe	-	Iron
FSS	-	Ferritic stainless steel
FZ	-	Fusion zone
GMAW	-	Gas-metal arc welding
GTAW	-	Gas-tungsten arc welding
HAZ	-	Heat affected zone
HV	-	Vickers hardness
I	-	Current

MOO	-	Multi-objective optimization
MPa	-	Mega Pascal
Nb	-	Niobium
^{o}C	-	Degree Celsius
OPM	-	Optical microscope
PAW	-	Plasma arc welding
RSM	-	Response surface methodology
S	-	Speed
SAW	-	Submerged arc welding
SCC	-	Stress corrosion cracking
Si	-	Silicon
SMAW	-	Shielded metal arc welding
Ti	-	Titanium
TIG	-	Tungsten Inert Gas
V	-	Vanadium
γ	-	Gamma
δ	-	Delta

CHAPTER ONE

INTRODUCTION

Tungsten inert gas welding (TIG) is broadly utilized for joining alloy steels and stainless steels used in numerous fabrication industries (Vijayan, 2018). They are mostly used for joining components for constructions of variety of structures such as buildings, bridges, ships, offshore structures, boilers, storage tanks, pressure vessels, pipelines, automobiles, and railroad vehicles. Under the same welding conditions, TIG welding processes can produce improved mechanical properties as compared to gas metal arc welding (GMAW) processes (Ugla, 2018). This welding technique is capable of providing good quality weldments of materials as well as coating with superior properties compared to other arc welding processes (Bello *et al*., 2015; Ganesh *et al*. 2014).

Tungsten Inert Gas (TIG) welding is an arc welding process that produces coalescence of metals by heating them with an arc established between a non-consumable tungsten electrode and the work piece with or without filler metal depending on the thickness of the workpiece (Dauda *et al*., 2010; Lokesh *et al.,* 2015). TIG welding process produces high quality weld joints and is suitable for joining thin and medium thickness material like aluminum alloys and steels (CibiandThilagham, 2017). Tungsten inert gas welding is specifically designed for welding materials with minimum heat energy input (Bello *et al.,* 2013).During fabrication of stainless steel components or equipment, manufacturers usually employ tungsten inert gas welding process as the principal joining method. Since any metal, including stainless steels, may undergo certain structural changes during welding, it is therefore, necessary to minimize and prevent any deleterious effects that may occur by selecting the proper welding process and controlling the welding conditions (Sanjay *et al*., 2018).

Stainless steels are important class of materials developed for critical applications as found in corrosive environments. These steels possess good corrosion resistance due to the formation of thin protective oxide layer on the surface (Ravinder and Jarial, 2015). They also exhibit better strength at high temperature, toughness at cryogenic temperature, and fabrication characteristics which makes their selection for industrial applications very popular. They are used for the demanding requirements of chemical processing to the delicate handling of food and pharmaceuticals (Amudaand Mridha, 2012).

Ferritic stainless steel (FSS) is a class of stainless steels with body-centered cubic crystal structure (BCC) having chromium content usually in the range of 11–27wt% (Balasubramanian *et.al.,* 2008; Amudaand Mridha., 2016). These steels have good resistance to stress corrosion cracking (SCC), pitting corrosion and crevice corrosion particularly in aggressive environments (Sanjay *et al*., 2018). They exhibit good ductility, formability, and moderately better yield strength relative to those of the austenitic grades, but the high temperature strength has been reported to be poor (Amudaand Mridha., 2011). One major problem that limits the industrial application of FSS is the loss of properties such as strength, hardness and impact energy in the weld section due to the intense welding heat input that induces grain coarsening. Katundi *et al*., (2010) reported that grain growth in the fusion zone (FZ) and heat affected zone (HAZ) occur due to high temperature gradient experienced by the component during welding. However, it may be possible to improve the strength and the toughness of a fusion welded FSS if refined grain structure is produced in the microstructure (Amudaand Mridha., 2010). Therefore, the present study is aimed at investigating the influence of TIG process parameters on the microstructure and some mechanical properties of AISI 430 ferritic stainless steel weldments.

1.1 Background of Study

Welding has been known as one of the permanent methods of joining materials together. Depending on the area of application, there are so many types of welding techniques known today, among which arc welding processes are the most popular. Tungsten inert gas welding is a type of arc welding process generally used for welding of stainless steels and other light materials because it offers low heat energy input into the weld joint which prevent the metal from excessive oxidation while in molten state. It is used for repair and maintenance in most industries such oil and gas as well as pipelines industries.

Ferritic stainless steels which is a type of stainless steels is becoming popular in this critical industry due to their excellent combined mechanical and chemical stability. In addition, they are less expensive compared to other types of stainless steels such as austenitic and martensitic.

However, they have some weldability problems that need to be address for their full-scale industrial applications.

1.2 Statement of Research Problem

Ferritic stainless steels are increasingly used to replace austenitic stainless steels in most critical industries such as oil and gas industry, pipeline industry, automobile industry etc. due to their excellent resistance to stress corrosion cracking (SCC) in alkaline and acidic environment and less expensive when compared to the austenitic counterpart (Amudaand Mridha, 2010). The principal welding issue with ferritic stainless steel is the grain growth in the fusion and heat affected zones due to the high heat input to the welded joint, which leads to the grain coarsening on solidification. This grain growth in the weldment lowers the mechanical properties of the material; therefore, limit their industrial application (Lokesh *et al.*, 2015).

In order to improve the mechanical properties of the weld joint, several techniques have been explored by different researchers to control the grain size of the weld. Mallaiah*et al*. (2014) used elemental powder addition and reported that, joint fabricated with addition of 2.0 g of titanium gives better mechanical properties due to refined grain structures obtained at that composition. Amuda and Mridha (2010) also reported that the most effective technique so far for the grain refinement of AISI 430 FSS is application of pulse AC-TIG welding which can produce weld with mechanical properties equivalent to 65% of the base metal. Also, extensive review of relevant literature shows that there were limited studies on the effect of welding parameters such as the welding current (I), the travel speed (S) and argon flow rate (AFR) on the hardness and tensile strength of ferritic stainless steel welds, which is the main thrust of the present research

In essence, this research focuses on the study of TIG welding parameters selection based on response surface methodology approach to achieve the goal of controlling the heat input and refining the grain structures for the attainment of enhanced mechanical properties in ferritic stainless steel welds.

1.3 Aim and Objectives

The aim of this research is to investigate the effect of TIG process parameters on the hardness, tensile strength and microstructure of AISI430 ferritic stainless steel welds. The specific objectives are:

i. to weld ferritic stainless steel at different TIG welding parameter levels based on central composite experimental design

ii. to characterize the surface topography and microstructural features of FSS weld zones

iii. to optimize the TIG welding parameters using CCD analysis to achieve the optimum values of the hardness and tensile strength of the FSS welds

iv. to develop mathematical model for the optimization process and validate the performance of the welding parameters at the optimal condition and then compare with that of the base metal

1.4 Scope of the Study

i. Welding of ferritic stainless steel using TIG welding process at different parameter levels.

ii. Evaluation of the macro and microstructures of the welded zones

iii. Determination of hardness and tensile strength of the welded samples using Vickers microhardness testing machine and Hounsfield tensometer respectively.

iv. Comparison between the optimized weld properties with the base metal

1.5 Justification of the Study

Ferritic stainless steels have moderate mechanical properties and good corrosion resistance. They are relatively cheap when compared to other grades of stainless steel. However, they have weldability problems due to grain coarsening in FZ and HAZ of the welds. The lower cost of ferritic stainless steels and the need for alternative materials that can sufficiently replace austenitic steels in terms of strength, toughness, resistance to corrosion is the driving force of this work.

CHAPTER TWO

LITERATURE REVIEW

2.1 Steels

Steels are alloys of iron and carbon with other trace elements such as sulphur, phosphorous, silicon, titanium, chromium, manganese, nickel, molybdenum etc. with carbon content within the range of 0.002-2.1% (Rajput, 2013). By controlling the amount of impurities and introducing additional alloying elements, wide range of steel products can be achieved with different physical, chemical and mechanical properties (Higgins, 2004).

2.2 Classification of Steels

2.2.1 Plain carbon steels

Plain carbon steels are iron-carbon alloys in which the properties are primarily derived from the presence of carbon with the presence of some incidental elements like manganese, silicon, sulphur and phosphorus in small amounts due to the method of making steels. The weldability and other characteristics exhibited by these steels depend primarily on the carbon content, although the alloying and residual elements do have some minor influences (Bob, 2003).

2.2.2 Carbon steels

a Low carbon steel

Low carbon steels, sometimes known as mild steels, have less than 0.30 percent carbon and are the most commonly used grades. They have good machinability, easily weldable and have better ductility than high carbon steels (Bob, 2003).

b Medium carbon steel

Medium-carbon steels contain 0.30 - 0.54%C. Increase in carbon content leads to higher mechanical properties such as hardness and tensile strength, however, the ductility is

reduced and it is more difficult to machine when compared to low carbon steels (Bob, 2003).

c High carbon steel

High carbon steels with carbon content between 0.54-0.75%C, have poor weldability. Hence, preheating, post heating and sometimes even heating during welding become necessary to produce acceptable welds and to control the mechanical properties of the steel after welding (Bob, 2003).

d Very high carbon steel

These contain carbon up to 1.50%C and are used for hard steel products such as metal cutting tools and truck springs. Like high-carbon steels, they require heat treating before, during, and after welding to maintain their mechanical properties (Bob, 2003).

2.3 Low-Alloy Steels

For welded applications, the carbon content of these steels is usually between 0.15- 0.25% and typical alloying elements include nickel, chromium, molybdenum, manganese, vanadium, titanium and silicon, which add strength at room temperature and increase low-temperature notch toughness. These alloy elements, when added in the right combination, improve corrosion resistance and influence the steel's response to heat treatment, but may also have negative influence on the crack susceptibility of the steel. Therefore, it is very important to use low-hydrogen welding processes with them. Preheating might also prove necessary. The preheating temperature depends on the carbon equivalent (CE) of the steel which can be determined by using the carbon equivalent formula shown in equation 2.1 (Dauda *et al.*, 2010).

$$\mathrm{C.E} = \%C + \frac{\%Mn}{6} + \frac{\%\mathrm{Cr} + \%\mathrm{Mo} + \%\mathrm{V}}{5} + \frac{\%\mathrm{Si} + \%\mathrm{Ni} + \%\mathrm{Cu}}{15}$$

2.1

2.4 Stainless Steels

Stainless steels are the most important commercial high-alloy steel used for several applications due to their ability to resist corrosion in aggressive environment. They have a chromium content of at least 10.5 % (Jurica, 2017), and some grades contain nickel in addition to chromium. Stainless steel possesses superior resistance to corrosion and high temperature oxidation (Kobe, 2015). It also has good workability as well as excellent mechanical properties at both low and elevated temperatures. Due to these advantages, stainless steels are used in various applications such as kitchen utensils, tableware, industrial machinery (for food processing, petroleum refinery, textile, fossil power, and nuclear power), building materials, and automobile components. Corrosion resistance of these alloy steels has been attributed to the presence of a thin layer of chromium oxide film which forms on the surface of a stainless steel and prevents it from further oxidation when exposed to corrosive conditions (Ravinder and Jarial, 2015). The major alloying elements that affect the metallurgical characteristics of these steels (such as the grain structures and the phases) are chromium, nickel, and carbon. Other alloying elements, such as molybdenum, niobium, titanium, manganese, nitrogen, and copper also contributed (Kobe steel, 2015). The common grades of wrought stainless steels are classified and assigned designations according to chemical composition. Table 2.1 shows the classification series for the three grades as classified by the American Iron and Steel Institute (Fisher and Maciag, 1977).

Table 2.2 gives the physical properties of various common grades of stainless steels, including those of carbon steel for comparison.

Table 2.1: Classifications of common-grade wrought stainless steels (AISI, 2015)

AISI classification series	Alloy type	Metallurgical phase
2XX	Cr-Ni-Mn	Austenitic
3XX	Cr-Ni	Austenitic

4XX	Cr	Ferritic & Martensitic

Table 2.2: Typical physical properties of common grades of stainless steels in comparison with carbon steel

Type of steel	Specific gravity	Electrical resistivity (μ Ω.cm)	Magnetism at room temperature (cal/g.^{o}C)	Specific heat at 0 -100.	Linear expansion coefficient at 0 -100. (10^{-6}/^{o}C)	Thermal conductivity at 100^{o}C (10^{-2}cal/cm/ sec^{o}C)
Carbon steel	7.86	15	Magnetic	0.12	11.4	11.2
Austenitic stainless steel (type 304)	7.93	72	Non-magnetic	0.12	17.3	3.89
Martensitic stainless steel (type 410)	7.75	57	Magnetic	0.11	9.9	5.95
Ferritic stainless steel (type 430)	7.70	60	Magnetic	0.11	10.4	6.24

(American Iron and Steel Institute, 2015)

2.4.1 Austenitic stainless steel

Austenitic stainless steel contains chromium, nickel, and manganese as the major alloying elements with the chromium contents generally above 16%, and nickel often between 5-7%. Austenitic stainless steels (Table 2.1) containing chromium and nickel as the principal alloying elements in addition to iron are identified as AISI 300 Series types. Those containing chromium, nickel, and manganese in addition to iron are identified as AISI 200 Series types. They can be hardened by cold working, but not by heat treatment. In the annealed condition, all are nonmagnetic, although some may become slightly magnetic by cold working. At room temperature the 300 and 200 Series stainless steels retain an austenitic microstructure (Roger, 2005).

While resistance to corrosion is their principal attribute, they are also selected for their excellent strength properties at high or extremely low temperatures. The chromium provides the oxidation and corrosion resistance while the nickel stabilizes the austenite phase sufficiently to retain most or all of it when rapidly cooled to room temperature. They are considered to be the most weldable of the high-alloy steels and can be welded by all fusion and resistance welding processes (Lakshman *et.al*., 2013).

2.4.2 Martensitic stainless steel

Martensitic stainless steels, which are identified by AISI 400 Series numbers (Table 2.1), contain chromium as the principal alloying element. In the annealed condition, these stainless steels have basically a ferritic microstructure and are magnetic. On heating beyond the critical temperature, the ferrite transforms into austenite. If then rapidly cooled to below the critical temperature, the austenite transforms into martensite. In many respects, the martensitic stainless steels are similar to the quenched and tempered carbon or alloy steels whose mechanical properties can be varied through heat treatment (Marcell, 2019). They have the least amount of chromium, offer high hardenability, and require both pre- and post-heating when welding to prevent cracking in the heat-affected zone (HAZ). Other alloying additions may also affect transformation. As a group, the martensitic stainless steels (hardenable by heat treatment) have certain characteristics in common which influence their behavior when subjected to the temperatures encountered in welding (Marcell, 2019).

2.4.3 Ferritic stainless steels

These are composed mainly of a body-centered cubic structure. Chromium (BCC) tends to stabilize α-Fe (BCC) and its high-temperature counterpart δ -Fe (BCC), which merge to form the so-called closed γ loop. It can be said that ferritic stainless steels have

metallurgical characteristics similar to those of Fe–Cr alloys containing sufficient (more than about 12%Cr) to remain outside the γ loop. They are essentially ferritic over the whole solid-state temperature range. To avoid forming an excessive amount of the brittle σ phase, however, the maximum Cr content of ferritic stainless steels is in general kept below 27% (Kou, 2003). On heating most ferritic stainless steel types above a critical temperature, the structure becomes austenitic which on cooling may partially transform into martensite (but not sufficiently to impart high strength). Consequently, ferritic stainless steels are considered not to be hardenable by heat treatment. Also, there will be a tendency for the ferrite grains to increase in size. These two structural features, (a) martensite formation and (b) grain growth, result in a reduction of ductility and toughness (Ghashemi*et al*., 2018).

2.4.3.1 Application of ferritic stainless steel

Ferritic stainless steel is considered very important in the family of stainless steels due to its high strength, better ductility and good corrosion resistance in chloride, acidic and petrochemical environment (Amuda and Mridha, 2009; Mridha and Amuda, 2011). Low thermal expansion, high heat conduction and resistance to stress corrosion are some important characteristics of ferritic stainless steel. Ferritic steel when compared with their counterpart family of stainless steels such as austenitic type, is more suitable for commercial use due to the absence of nickel, which makes it more economical (Santos *et.al*., 2012). Ferritic stainless steel is a Ferrous Chromium (Fe-Cr) base alloy. Due to their good machinability and formability, it is used in fabrication of different useful products. The coefficient of thermal expansion of ferritic steel is low as compared to austenitic steel which makes it more useful in high temperature environment (Ramkumar *et.al*., 2015; Sabioni*et.al*., 2003). Ferritic stainless steel is a candidate material in less severe corrosion atmosphere for chemical processing equipment, furnace parts, heat exchangers, petroleum

refining equipment, recuperators, storage vessels, electrical appliances, solar water heaters, and household appliances. They are particularly more appropriate in alkaline and chloride environments (Amuda and Mridha, 2009).

2.5 Microstructure of Steels

Steels undergo different microstructural transformation when subjected to dynamic heating and cooling processes. Some of the common microstructures resulting from steel transformation includes austenite, martensite, bainite, pearlite, cementite and ferrite structures. These structures exist at different temperature ranges and make the steel to poses different properties such as the strength, hardness, toughness etc(Kou, 2003). some of these microstructures present in steels are presented in Figure 2.1.

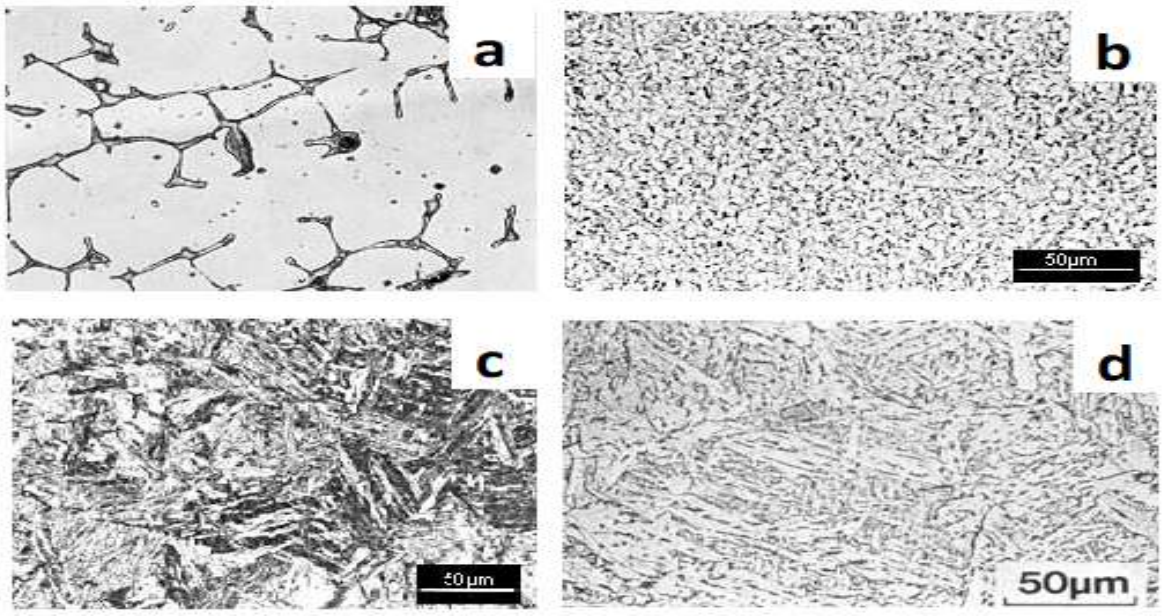


Figure 2.1: Some microstructures of Steel (a) austenite structure(b) ferrite structure (c) pearlite structure (d) martensite structure (Kou, 2003)

2.6 Fusion Welding Process

Fusion welding processes are all those welding processes where faying surfaces of parent parts as well as filler materials are made molten during welding for weld bead formation. Heat is always associated with these processes without the application of external pressure

except for resistance welding group which requires substantial contact pressure to be maintained during welding for sound joining. Filler material may or may not be applied during fusion welding (Dauda *et al*., 2010).

Fusion welding process is the most widely used welding processes for fabrication, repairs and maintenance in different fields of engineering applications. There exist a large number of fusion welding processes and the same can be further grouped on the basis of source of heat. Such processes where heat is applied by means of electric arc are termed as arc welding processes. Also, gas welding processes, high intense energy welding processes and resistant welding processes, are basically examples of fusion welding (Dauda *et al*., 2010).

Arc welding (Figure 2.2) is one of several fusion welding processes used for joining metals by applying heat at the joint created between the two parts which melted and fused together, or more commonly, with an intermediate molten filler metal. In arc welding, the intense heat needed to melt metal is produced by an electric arc. The arc is formed between the workpiece and the electrode (stick or wire) which is either manually or mechanically guided along the joint to be welded. The electrode can either be a rod with the purpose of simply carrying the current between the tip and the work such as gas tungsten arc welding (GTAW) and plasma arc welding (PAW), or it may be a specially prepared rod or wire that not only conducts the current but also melts and supplies filler metal to the weld joint (shielded metal arc welding, gas metal arc welding, flux-cored arc welding etc.). Most welding processes in the manufacture of steel products use the second condition where the filler metals melted and filled the weld joint (Bolarinwa*et al.* 2018).

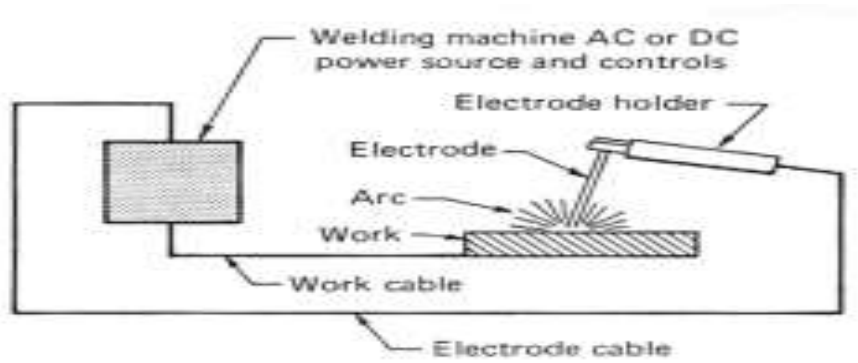


Figure 2.2: Basic arc welding circuit diagram(Kou, 2003)

2.6.1 Shielded metal arc welding process (SMAW)

This arc welding process employ covered or coated electrode to create an arc which is the heat source for the welding process. The coatings, during welding, decompose and provide the necessary shield which protects the molten metal from the atmospheric oxygen and nitrogen. Shielded metal arc welding popularly referred to as stick or manual metal arc welding is the oldest and most commonly used welding process in the world (Penuela*et al.*, 2009 and Dauda *et al*., 2010).

Shielded Metal Arc welding uses the heat of the arc generated to melt the base metal and the tip of a consumable covered electrode. Both the electrode and the work are part of an electric circuit. This circuit begins with the electric power source and includes the welding cables, an electrode holder, a workpiece connection cable, the workpiece (weldment), and an arc welding electrode. One of the two cables from the power source is attached to the work while the other is attached to the electrode holder as shown in Figure 2.3

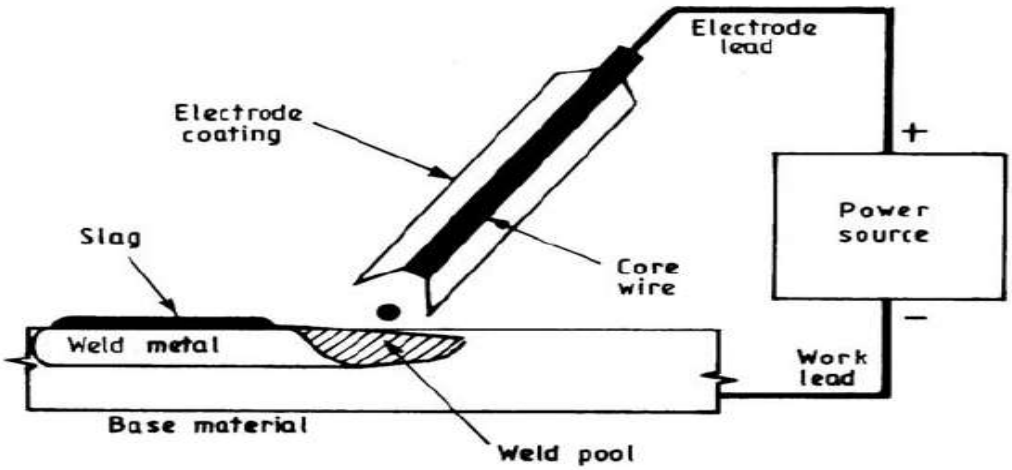


Figure 2.3: Shielded metal arc welding process(Kou, 2003)

2.6.2 Gas-metal arc welding process

Gas–metal arc welding (GMAW) is a welding process that causes the coalescence of the metal surfaces to be joined by heating them with an arc produced between a continuously fed filler wire electrode and the metals, as shown in Figure 2.4. Shielding of the arc and the molten weld pool is often obtained by using inert gases such as argon and helium or active gases such as carbon dioxide, oxygen, nitrogen or their mixture (Kou, 2003). Depending on the type of shielding gases employed, gas metal arc welding process can be referred to as metal- inert gas (when inert gases are used) or metal-active gas (when active gases are used). During the welding process, the arc is struck by direct contact between the wire electrode and the workpiece and maintained at a constant length by the interaction of the electrical parameters. The wire electrode which is wound round a spool is fed continuously through the welding torch at a preset speed. It is an all-position semi-automatic welding process, though the automatic version is also available in some advanced countries (Richard, 2012).

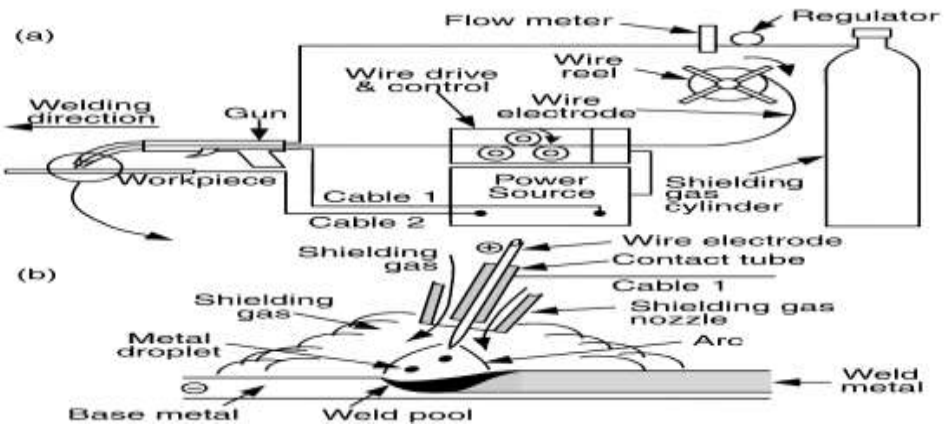


Figure 2.4: Gas-Metal Arc Welding Process (Kou, 2003)

2.6.3 Tungsten inert gas welding process

Gas-tungsten arc welding (GTAW) or tungsten inert gas welding (TIG) is a welding process that melts and joins metals by heating them with an arc established between a non-consumable tungsten electrode and the metals. The torch holding the tungsten electrode is connected to a shielding gas cylinder as well as one terminal of the power source, as shown in Figure 2.5. The tungsten electrode is usually in contact with a water-cooled copper tube, called the contact tube, which is connected to the welding cable from the terminal. This allows both the welding current from the power source to enter the electrode and the electrode to be cooled to prevent overheating. The workpiece is connected to the other terminal of the power source through a different cable. The shielding gas goes through the torch body and is directed by a nozzle toward the weld pool to protect it from the air. Protection from the air is much better in GTAW than in SMAW because an inert gas such as argon or helium is usually used as the shielding gas and because the shielding gas is directed toward the weld pool (Kou, 2003).

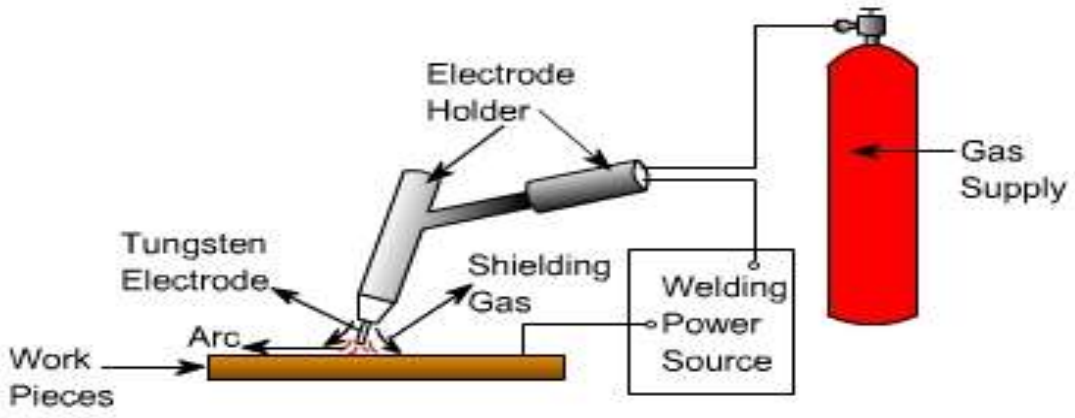


Figure 2.5: Gas-Tungsten Arc Welding Process (Kou, 2003)

a. Process parameters in TIG welding

The common process parameters to be considered during TIG welding include; the welding current, travel speed, welding voltage and argon flow rate. However, welding voltage and argon flow rate have been reported to have little effect on the net heat input to the weld joint (Amuda and Mridha, 2010). The relationship between the heat input and the process parameters is given in equation 2.2

Heat input (HI) = $\frac{VI}{S}$ 2.2

Where V, I and S are the welding current (A), arc voltage (V) and travel speed (mm/s) respectively.

b. Welding current

Welding current is one of the most important factors considered during TIG welding process. It is the most influential variable in arc welding processes which controls the electrode burn off rate, the depth of fusion and geometry of the weldments (Bolarinwa*et al.* 2018). Depending on the types of workpiece and the tungsten electrode used, there are three choices of welding current in TIG welding, these are: Direct Current electrode negative (DCEN or straight polarity), direct Current electrode positive (DCEP or Reverse

Polarity) and Alternating Current with High Frequency stabilization. Each of these current choices has its advantages and disadvantages. A look at each type and its uses will help the operator select the best current type for the job. The type of current used will have a great effect on the penetration pattern as well as the weld bead configuration. Figure 2.6 shows the arc characteristics of each current type.

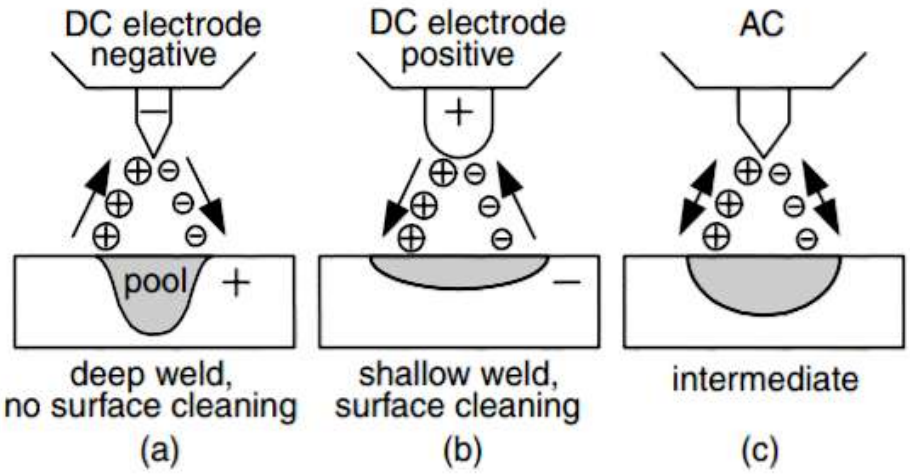


Figure 2.6: Three different current polarities in TIG Welding (Kou, 2003)

c. Welding speed

Welding speed is another important factor considered during welding process. Ahmed *et al.* (2010) reported that a very high welding speed results in a poor weld bead penetration, hence; reducing the tensile property of the welded joint. On the other hand, when the welding speed is very slow, too much heat will be concentrated at the welded zone, resulting in a coarse grain in the re-solidified weldment. Therefore, it is necessary to select an optimum welding speed that will produce weld joint with adequate mechanical properties.

2.7 Welding of Stainless Steels

Stainless steels are widely used in various industries because of their excellent resistance to corrosion. The welding of stainless steels, especially the austenitic grades, is important

in energy-related systems, for instance, power generation and petrochemical refining systems (Kou, 2003). During the welding of stainless steels, the temperatures of the base metal adjacent to the weld reach levels at which microstructural transformations occur. The degree to which these changes occur, and their effect on the finished weldment, in terms of resistance to corrosion and mechanical properties, depends upon the heat input, alloy content, thickness, filler metal, joint design, weld method, and welder skill. Regardless of the changes that take place, the principal objective in welding stainless steels is to provide a sound joint with qualities equal to or better than those of the base metal, allowing for any metallurgical changes that take place in the base metal adjacent to the weld and any differences in the weld filler metal. In welding, there are three zones of principal concern: (1) The solidified weld metal, composed of either base metal or base metal and filler metal; (2) the heat affected zone (HAZ) in which the base metal is heated to high temperatures but less than the melting temperature; and (3) the base metal which is only moderately warmed or not warmed at all. The three zones are illustrated in Figure 2.7.

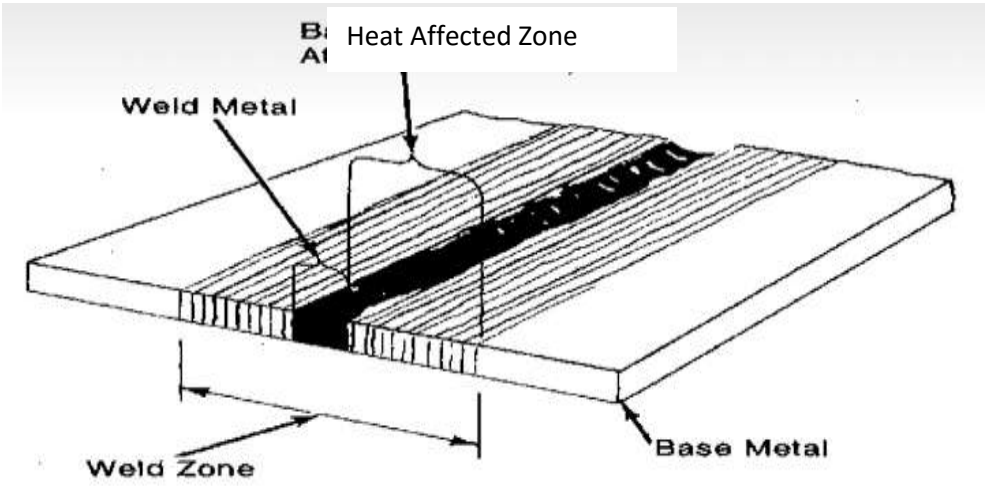


Figure 2.7: Thermal affected areas of metal due to welding (Kobe Steel, 2015)

2.7.1 Welding of austenitic stainless steel

Austenitic stainless steel is considered to be the most weldable of the high-alloy steels and can be welded by all fusion and resistance welding processes. They are readily joined by

arc welding, resistance welding, friction welding, electron beam and laser beam welding process (Lakshman *et.al*., 2013; Parmer, 2010). The common arc welding processes used for joining austenitic stainless steels are shielded metal arc welding (SMAW), gas metal arc welding (GTAW), submerged arc welding (SAW) and Plasma arc welding (PAW). In comparison with mild steel, for example, the austenitic stainless steels have several characteristics that require some revision of welding procedures that are considered standard for mild steel. Austenitic stainless steels offer excellent weldability, but austenite isn't stable at room temperature. Consequently, specific alloys must be added to stabilize austenite. The most important austenite stabilizer is nickel, and others include carbon, manganese, and nitrogen. Special properties, including corrosion resistance, oxidation resistance, and strength at high temperatures, can be incorporated into austenitic stainless steels by adding certain alloys like chromium, nickel, molybdenum, nitrogen, titanium, and columbium. And while carbon can add strength at high temperatures, it can also reduce corrosion resistance by forming a compound with chromium. It is important to note that austenitic alloys cannot be hardened by heat treatment. That means they do not harden in the weld heat affected zone.

The melting point of the austenitic grades is lower, so less heat is required to produce fusion. As previously illustrated in Table 2.2, their electrical resistance is higher than that of mild steel so less electrical current (lower heat settings) is required for welding. These stainless steels also have a lower coefficient of thermal conductivity, which causes a tendency for heat to concentrate in a small zone adjacent to the weld. The austenitic stainless steels also have coefficients of thermal expansion approximately 50% greater than ferritic stainless steel, which calls for more attention to the control of warpage and distortion during welding (Mike, 2007).

2.7.2 Welding of martensitic stainless steel

Typical martensitic stainless steels are Types 410 and 403 containing 13%Cr. Unlike austenitic stainless steels, martensitic stainless steels have a transformation point at around 800-850^{o}C. Therefore, heating this steel at high temperatures in the range above this transformation point, followed by air cooling, causes the transformation of austenite to martensite having very high hardness. In welding this type of steel, the microstructures of the HAZ become quenched martensite with a very hard and brittle structure having Vickers hardness over 300 HV. Therefore, cracking is likely to occur in the welds. In order to prevent the cracking, the control of preheating temperatures (200-400^{o}C) is necessary. Postweld heat treatment (PWHT) is also necessary to temper the postweld martensitic structure, thereby improving the mechanical properties of the weld metal and HAZ (Kobe steel, 2015).

2.7.3 Welding of ferritic stainless steel

Ferritic stainless steels, although generally considered less weldable than austenitic stainless steels, have advantages such as lower costs and better resistance to stress corrosion cracking than austenitic stainless steels. The most commonly used ferritic stainless steel perhaps is the AISI430 type, which usually contains about 17%Cr and 0.05-0.12%C. During welding, rapid cooling from temperatures above 700ºC may cause intergranular precipitation (similar to carbide precipitation in austenitic stainless steels) that result in reduced resistance to corrosion. Consequently, the AISI numbered ferritic stainless steels are not considered attractive from the standpoint of weldability (Kobe steel, 2015). These steels are ferritic at all temperatures below the melting point showing no transformations to austenite or martensite. As is typical of ferritic grades they are susceptible to grain growth, but at a lower carbon levels, the toughness of these grades is significantly higher than the standard grades (Kobe steel, 2015).

a. Grain growth and martensite formation in ferritic stainless steels

Figure 2.8 shows the microstructure of AISI 430 ferritic stainless steel in the base metal, FZ and the HAZ (Kou, 2003). Micrograph *b* (away from the fusion boundary) reaches the austenite formation ranges ($\delta + \gamma + C_1$ and $\delta + \gamma$) of the phase diagram (Figure 2.8 (a)). Here, austenite formed along grain boundaries and, due to fast cooling during welding, the austenite transformed into martensite (Figure 2.8*b*) with little grain growth. Position *a* (near the fusion boundary), on the other hand, reaches the δ -ferrite range and excessive grain growth takes placeat high temperatures (Figure 2.8*a*). During cooling through the austenite formation ranges, a considerable amount of austenite formed at the grain boundaries. The austenite appears needlelike because of the large grain sizeand the high cooling rate. During further rapid cooling to room temperature, the austenite transforms into needlelike martensite. Because of excessive grain coarsening and formation of needlelike martensite at grain boundaries, the notch toughness of as-welded AISI 430 stainless steel is poor. Post weld heat treatment at 800°C (martensite tempering) significantly improves the notch toughness. Suppressing martensite formation by adding 0.5% Ti or 1% Nb also helps (Castro and De Cadenet, 1974). This is probably because both Ti and Nb increase the stability of delta-ferrite, thus suppressing the formation of austenite. Furthermore, as mentioned previously, they tend to form carbides at high temperatures. Therefore, the carbon content is reduced and the tendency to form martensite decreases. Excessive grain growth can be avoided by using lower welding heat inputs. It has also been suggested that nitride and carbide formers such as boron, aluminium, vanadium, and zirconium can be added to ferritic stainless steels to suppress grain growth during welding (Amuda and Mridha, 2011).

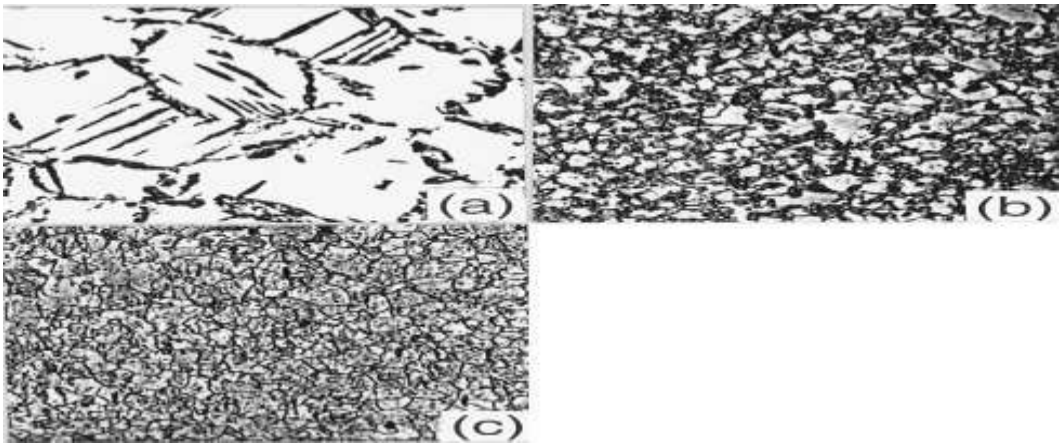


Figure 2.8: Microstructure of AISI 430 stainless steel (magnification 212X): (*a*) near fusion boundary; (*b*) near base metal; (*c*) base metal (Kou, 2003).

b. Problems with ferritic stainless steel weld

Figure 2.9 describes the phase structures which ferritic stainless steel undergoes at a given temperature and at a given carbon and nitrogen content. Low chromium ferritic fall into outer gamma-loop, where the phase structure is dual phased with majority being ferrite and substantial amount of austenite as shown in Figure 2.9(a). Medium chromium steels can either have a dual phase or fully ferritic structure as the carbon and nitrogen content widen the gamma-loop size as shown in Figure 2.9(b). During welding of ferritic stainless steels, there is always a problem of grain coarsening in the heat-affected zone and weld metal because they solidify directly from the liquid to the ferrite phase without any intermediate phase transformation, especially high-chromium ferritic stainless steel (Villafuerte *et.al*., 1990) as shown in Figure 2.9. These problems have been reported in different journals, and several approaches have been explored by many researchers in order to find solutions to the problems (Mridha and Amuda, 2011).

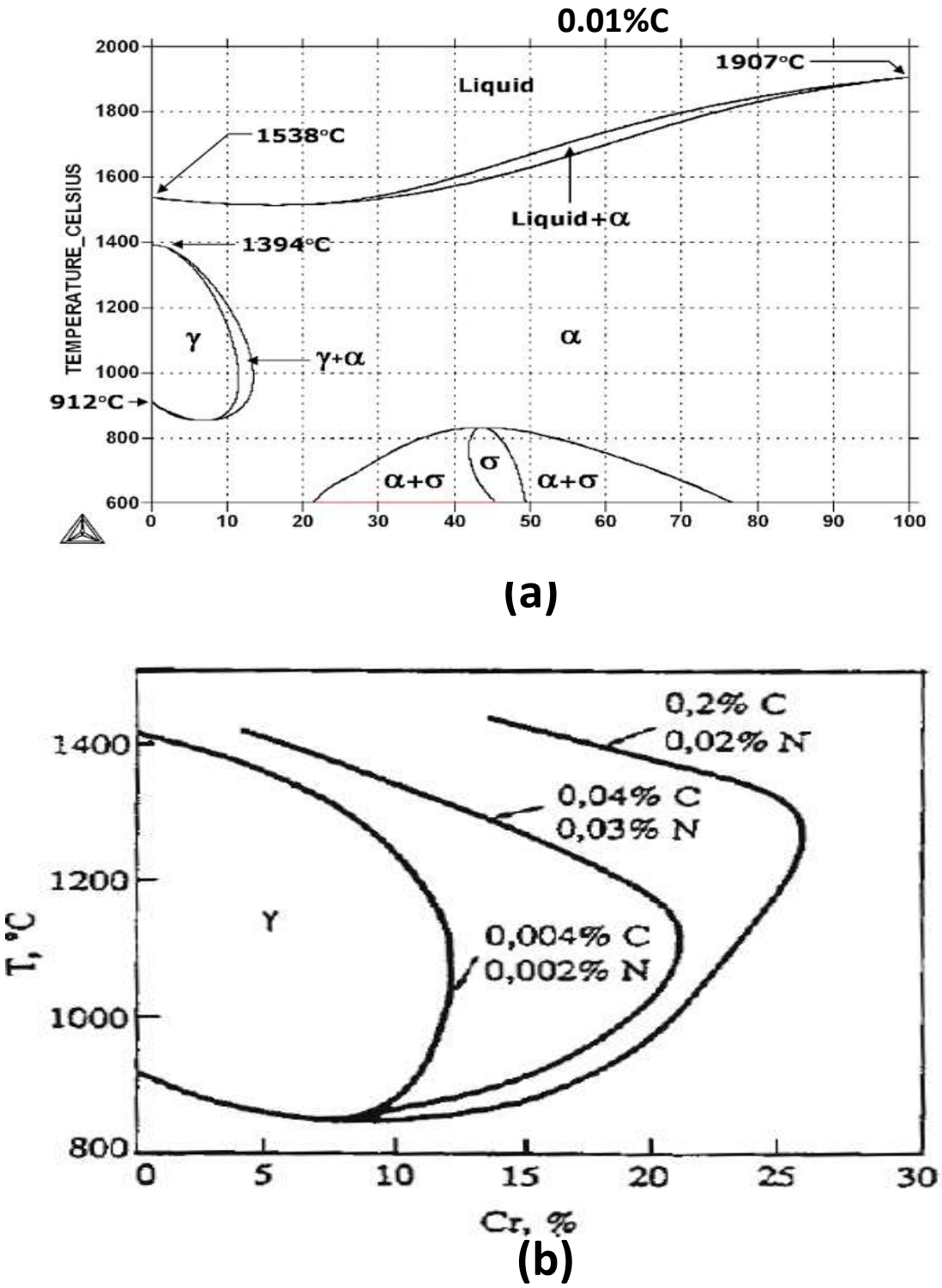


Figure 2.9: Vertical section of Fe–Cr–C phase diagram (a)showing wt.% Cr at 0.01%C (b) showing the influence of C and N on the gamma-loop. Castro and De Cadenet (1974).

2.8 Design of Experiment Techniques

Design of experiment is a systematic process of planning, designing, and analyzing the experiment in order to obtain valid and objective conclusions. It involves integration of simple and powerful statistical method so that sound conclusions can be drawn from the

experiment (Adebisi 2016). The success of any design experiment depends on proper planning, appropriate choice of design and the method of statistical analysis employed. In tungsten inert gas welding, the factors usually considered are the welding current, welding voltage, travel speed and sometimes, the argon flow rate. It is therefore, necessary to utilize optimization process that depends on the analysis of those parameters to determine their contributing effects on the final welds (Adebisi 2016).

2.8.1 Factorial design

Factorial design is one of the most important methods used to determine the effects of multiple variables on a response. Traditionally, experiments were designed to determine the effect of one variable upon one response. Factorial design has the advantages of reducing the number of experiments to perform by studying the multiple factors simultaneously. According to Fisher (1992), there are some advantages when the study of multiple variables in the same factorial experiment is being combined. Moreover, factorial design can be used to determine both the main effect and the interaction effects

2.8.2 Response surface methodology

In statistics, response surface methodology is used to explore the relationship among several variables and one or more response variable. This statistical method was introduced. The main idea of this model is to use a sequence of designed experiments to obtain an optimal response. Box and Wilson (1951) suggested using a quadratic model to do this. They acknowledge that this model is only an approximation, but it is easy to estimate and apply, even when little is known about the process.

Statistical approaches such as RSM is a mathematical tool used to plan, develop and maximize the production of a special substance by optimization of operational variables. In contrast to conventional methods, the interaction among process variables can be determined by statistical techniques. Response surface methodology is applicable to

situation where several input factors affect the response performance. Central composite design (CCD) and Box-Behnken design (BBD) are the two common methods of RSM, however, central composite design is most commonly used due to its flexibility, high quality prediction and its rotatability compared to other types of design. The following are some of the advantages of Response Surface Methodology (Adebisi 2016).

i. Orthogonality: This property allows individual effects of the n-factors on the responses to be estimated independently
ii. Rotatability: The property of rotating points of the design about the center of the factor space. The moments of the distribution of the design points are constant.
iii. Uniformity: A third property of CCD designs used to control the number of center points is uniform precision (or Uniformity).

a. Central composite design

Central Composite Design (CCD) involves sequential steps of experimentation with 2^n factorial points augmented by additional central and 2n star or axial points. Factorial points provide linear estimation and interaction terms, while the star points and center run gave the presence of curvature and error respectively (Diler and Ipek, 2012). Because of the rotatability of CCD, it is capable of providing an equal precision of estimation in all direction. Considering a factorial point of each factor ±1 unit away from the center of the design region, the axial (star) points will be given as ±α such that $|\alpha| > 1$. The value of α depends on the number of the input factors and other properties. For a rotatable design and full factorial experiment, α can be estimated using equation 2.3 (Diler and Ipek, 2012).

$$\alpha = (2^n)^{1/4} \quad 2.3$$

Where n is the number of input factors

b. Box-Behnken design

Box-Behnken design is another type of response surface design that does not contain an embedded factorial or fractional design. It is the second most popular method used for fitting a second order polynomial model. While CCD consists of five levels ($-\alpha$, -1, 0, +1, $+\alpha$), Box and Behnken (1960) developed a three levels design (-1, 0, +1) that allows the estimation of the general quadratic model (John, 2014). these designs consist of 2^2 factorials in each pair of factors with all other factors held constant at their mid-level with a few center points. Box-Behnken design cannot be used when only two input factors are involved. Some of the advantages of BBD over CCD are that it is less costly and requires less total experimental runs. However, it cannot be built up in two steps starting with a 2^n design.

2.9 Central Composite Design Optimization Tools

In order to perform the analysis and optimization of experimental results using central composite design, the results were normallyanalyzedusingthestatisticaloptimizationtoolssuchasANOVA,fitsummary and regression analysis, Box-Cox transform and all other validation and adequacy tools.

2.9.1 Analysis of Variance (ANOVA)

Analysis of variance (ANOVA) is a statistical tool used to analyze and determine the influence that independent variables have on the dependent variable in a regression study. It allows a comparison of more than two groups of parameters at the same time to determine whether a relationship exists between them.

2.9.2. Fit summary Statistics

The fit summary statistics normally presents the appropriate models to fit the experimental data into first-order, second-order, linear with interactions and cubic polynomial (Myers *et al.,* 2009). It analyses the relationship between the independent variables (factors) and the selected response

2.9.3 Box-Cox Transform

The Box-Cox transform the non-normal dependent variable into a normal shape. The curve preforms data analysis on the response factor by providing a confidence interval on the transformation parameter (Lambda) based on the result. The analysis is normally performed to show whether or not a transformation is needed. Transformations are normally performed when there is need to normalize the dependent variable or stabilize the variance in order to improve the model (Adebisi, 2016), This usually occur when the confidence level is not unity. It transforms the non-normal dependent variable into a normal shape. The curve preforms data analysis on the response factor by providing a confidence interval on the transformation parameter (Lambda) based on the result obtained.

2.10 Summary of Major Findings on Stainless Steel Welds

Subhas *et al*. (2019)carried out an investigation on the effects of TIG welding parameters on microstructures and mechanical properties of AISI 316L stainless steel using responsesurface methodology approach and concluded that the optimized UTS of 641.55 MPa, impact strength of 50.87J and weld width of 6.26 mm were obtained at a current =129.29 A, speed =16.85 cm/min and gas flow rate = 8.91 cm/min.

Vidyarthy*et al*. (2017)performedoptimization of A-TIG process parameter using surface response methodology on different aspect of weld bead geometries of ferritic stainless steel welds. The results obtained shows that the optimized depth of penetration (DP) and depth to width ratio (D/W) were 6.95mm and 0.80mm respectively at a Current of 213.78A, speed of 96.22mm/min and 1.99mg/cm^2 flux coating density.

Sanjay *et al.* (2017)worked on optimization of TIG welding process parameters using Taguchi's analysis and response surface methodology to evaluate the bending strength and microhardness of AISI 304 Austenitic stainless steel and concluded that the optimum

properties were obtained at 70 A welding current, 50 V arc voltage, 0.5 mm root gap and gas flow rate of 16 litter/min .

Anbazhagan and Nagalakshmi (2002) studied grain refinement of AISI 430 FSS weld using constant and pulsed current TIG as well as shielded metal arc (SMAW) process. They established that pulsed current TIG offers appreciable grain refinement in the weld leading to about 60% increase in ductility. The SMAW process with E430Nb electrode gave 40% improvement in ductility.

Amudaand Mridha (2012) used both cryogenic cooling and elemental metal powder addition to evaluate and compare the degree of grain refinement of AISI 430 ferritic stainless steel and concluded that the two strategies provided equiaxed and refined grain structures in the re-solidified weld pools. But, the addition of elemental powder produced more equiaxed and refined grain structure than the cryogenic cooling.

Pekkarinen and Kujanpää (2010) determined empirically, the microstructural changes in FSS by controlling the heat input parameters in laser welds. The study concluded that martensite formation and grain size of ferritic stainless steel is much dependent on welding parameters. With low heat input, there was almost no martensite and the grain size was large. Increasing heat input, leads to increase in the amount of martensite formation with a decreased in the grain size.

Lakshminarayanan*et al*. (2009) investigated the effect of different welding processes such as shielded metal arc welding (SMAW), gas metal arc welding (GMAW) and tungsten inert gas welding (TIG) on tensile and impact properties of AISI 409M FSS welded joints. They found that joints produced by TIG have superior tensile and impact properties compared with SMAW and GMAW welded joints. This aspect was mainly due to the presence of finer grains in the weld metal and HAZ.

Mallaiah*et al*. (2014)investigated theinfluence of titanium (Ti) addition on the mechanical properties, residual stresses, and corrosion behavior of AISI 430 grade FSS weld and found that joint fabricated with addition of 2g titanium gives better mechanical properties due to a refined grain structure obtained at that composition.

Bensaid*et al*. (2012)performedoptimization of TIG welding parameters in ferritic stainless steel weld using Taguchi design approach and concluded that a minimum grain size of 183.26μm was obtained at an optimum welding parameter of 55A and 3.1mm/s for welding current and speed respectively.

Mohandas *et al*. (1999)carried out a comparative evaluation of GTAW and SMAW on the grain refinement of ferritic stainless steel welds and found that GTAW welds with equiaxed grain morphology gave better mechanical properties compared with SMAW

Sathiya*et al*. (2007) investigated the effect of friction stir welding parameters on the mechanical and metallurgical properties of ferritic stainless steel weld. The study found that about 95% property (tensile strength) of the base metal was achieved with fine grain structure.

A review on weldability of stainless steels has been carried out during the course of this study and the summary of the major findings is presented in section 2.9. It can be concluded that minimizing the heat energy input and improvement in the mechanical properties of stainless steel welds particularly ferritic stainless steels are of great concern among the researchers. Different techniques which have been explored by these researchers include; variation of the welding process parameters, elemental powder addition, cryogenic cooling method and the use of low heat energy input such as friction welding and TIG welding process to achieve this goal. The major research gap is the lack of investigation on the effect of TIG process parameters on the microstructures and mechanical properties of ferritic stainless steel welds. Based on literature studies, the

following TIG welding parameters (Current, speed and argon flow rate) were selected for the optimization process.

Therefore, the current study investigates the effects of TIG welding parameters on microstructural features and some mechanical properties of ferritic stainless steel welds through response surface methodology based on central composite design approach to achieve the aim of minimizing the heat input and improving the mechanical properties of FSS welds.

CHAPTER THREE

MATERIALS AND METHOD

3.1 Introduction

This chapter describes the experimental procedure as applied to the materials and equipment used in this investigation. The methodological design plan and data optimization analysis through response surface methodology was equally described. The experimental aspect involved the welding of the stainless steel (FSS) based on the design plan using autogenous tungsten inert gas welding process. The statistical approach

involved the use of central composite design aspect of the response surface methodology (RSM) for the design of experiment and optimization of the process.

3.2 Materials

The materials used in this study are AISI 430 FSS, different sizes of grit papers, hack saw, alumina polishing cloth, etchant, epoxy and argon gas

The ferritic stainless-steel sheet with dimensions of 1200mm (L) x 300mm (W) x 1.5mm (T) used in this study was purchased from CencoSains Company, Malaysia. The chemical composition was analyzed at JFE quality assurance section, East Japan works (China), and the inspection certificate is attached in appendix A. The chemical composition of the stainless steel is given in Table 3.1.

Element	C	Si	Mn	P	S	Cr	Fe
% composition	0.12	0.75	1.00	0.040	0.030	17	balance

Table 3.1: Chemical Composition of AISI 430 Ferritic Stainless Steel

3.2.1 Equipment

The equipment used in this research and the Laboratories were presented in Table 3.2

S/N	Name of equipment	Laboratory
1	TIG welding Machine	NLNG Lab, A.B.U- Zaria
2	Vicker's Microhardness Testing Machine	Shell Lab, A.B.U- Zaria
3	Tensile Testing Machine	Materials Testing Lab, Dept. of Mechanical Engineering, A.B.U- Zaria

4	Metallurgical Microscope	Metallographic Lab, Dept. of Met. & Mats. A.B.U- Zaria
5	Lathe Machine	Machining Lab, Dept. of Met. & Mats. A.B.U- Zaria
6	Polishing Machine	Metallographic Lab, Dept. of Met. & Mats. A.B.U- Zaria
7	Power cutting machine	Machining Lab, Dept. of Met. & Mats. A.B.U- Zaria

Table 3.2: Equipment and the Laboratory

3.3 Methodology

Figure 3.1 shows the experimental flow chart for the study which includes all the processes involved, starting from parameter selection, experimental design, conduction of the experiment, materials testing, result analysis through RSM design expert, validation and interpretation of the results.

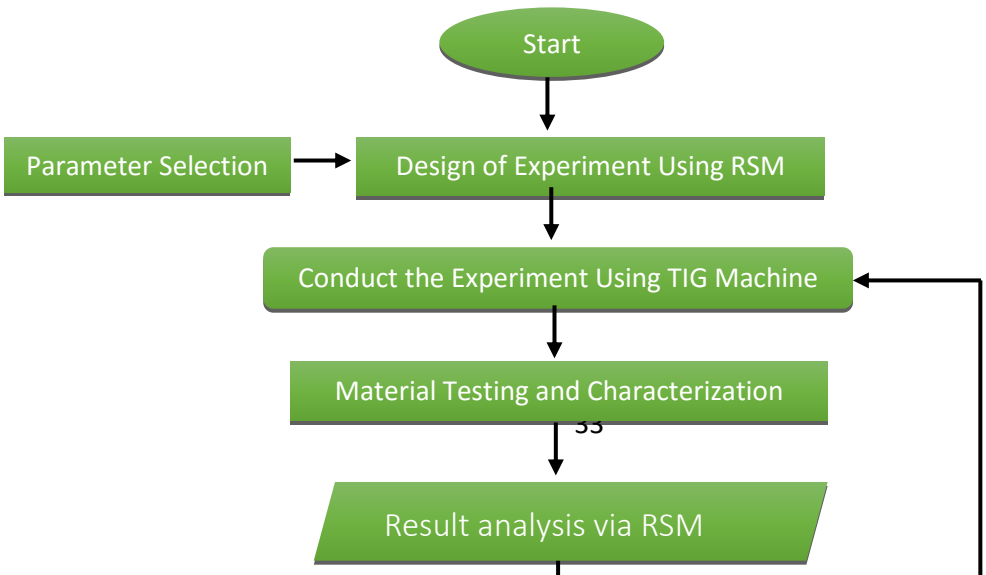


Figure 3.1: Experimental flow chart

3.3.1 Selection of input factors

The selection of input factors which can also be referred to as the processing parameters was based on extensive literature study as well as considering the most relevant variables with influential effect on TIG welding process. Preference is also given to the type and model of the TIG machine that was used for the study, i.e. the current and voltage rating of the machine as well as whether it is AC or DC machine. Based on this consideration, the following critical process parameters and their levels were chosen; the welding current (I), welding speed (S) and the argon flow rate (AF) as the input factors. Central composite design (CCD) was used to plan and design the experiment. This was varied over five levels ($-\alpha$, -1,0, +1, $+\alpha$) with three elements as factorial points, axial/star point and center runs. The factorial levels chosen for the current were 15A and 25A, while the values of 3mm/s and 5mm/s as well as 6L/min and 10L/min were selected for the speed and the argon flow rate respectively. The input factors and their levels are presented in Table 3.3.

Factors	Symbols	Levels				
Welding current (A)	*A*	10	15	20	25	30

Table 3.3: Factors and levels for the CCD experimental design plan

Welding speed (mm/s)	*B*	2	3	4	5	6
Argon flow rate (L/min)	*C*	4	6	8	10	12

3.3.2 Response variable for the study

Theresponse variable selected for this study are tensile strength and hardness, which were believed to be directly influenced by the input factors. The choice of these output factors depends on the intended area of application such as automobile industry, pipelines as well as oil and gas industries.

In addition, literature studies have shown that the responses (tensile strength and hardness) are one of the most important output factors used to evaluate the weld quality of autogenous TIG welding of alloy steels and stainless steels weldment.

3.3.3 Multi-Objective Optimization Process

In optimization analysis, it is important to employ the idea of multi-objective optimization (*MOO*) to locate a set of conditions which optimize two or more responses simultaneously or keep them within the desirable limit. The desired goal is usually set as either to maximize or minimize the responses within the input factor ranges. This implies that each of the responses has a defined goal of either minimization or maximization. In this study, the optimization interest was to achieved a set of tungsten inert gas welding process parameter conditions that gives maximum tensile strength and hardness. This individual response goal was combined into an overall desirability function and a search for optimal

solution through central composite design analysis was obtained, which provides the best parameter conditions that maximized the two responses simultaneously.

3.3.4 Experimental design matrix

Circumscribed type of central composite (CCC) design with three factors at five levels was chosen for the experimental design, and this represent the case of second-order modeling for the responses. The total number of experimental runs was estimated using $2^k + 2k + 6$, with 8 factorial points (2^k), 6-star points (2k) and 6 central runs to make up a total of 20 experimental runs as shown in Table 3.4, i.e. $2^3 + 2(3) + 6 = 8+6+6 = 20$ runs.

Where k is the number of input factors, and the central run is chosen as six (6) for convenience and accuracy especially when the input factors is more than two (Adebisi 2016).

Experimental Run	Factors			Responses	
	A: Welding Current (A)	B: Welding Speed (mm/s)	C: Argon Flow Rate (L/min)	Tensile Strength (MPa)	Hardness (HV)
1	15	3	10		
2	20	4	8		
3	20	4	8		
4	15	5	10		
5	15	3	6		
6	25	3	10		
7	20	4	8		
8	20	6	8		
9	10	4	8		
10	25	3	6		
11	20	4	12		
12	20	2	8		
13	20	4	8		
14	30	4	8		
15	15	5	6		
16	25	5	6		
17	20	4	8		
18	25	5	10		
19	20	4	8		
20	20	4	4		

Table 3.4: Design matrix of process parameters for TIG welding process

3.4 TIG Torch Welding Technique.

Clarke 101 Inverter TIG torch welding techniques shown in Figure 3.2 was selected for the welding of FSS in this investigation. In this process, direct current electrode negative (DCEN) also known as straight polarity was used for the autogenous TIG welding. The TIG welding machine used non-consumable tungsten electrode which contains 2% thorium and 2.5mm tip diameter. Pure argon gas was used as the shielding gas at variable flow rates with the help of flow meter.



Figure 3.2: TIG welding machine set-up

The sample (AISI 430 FSS) in sheet form with thickness 1.5mm was cut into a dimension of 120mm x 90mm using a cutting machine. It was then cut into two equal parts along the width and then butt weld using TIG welding process. After welding, tensile and hardness

test samples were cut from each of the welded samples across the weldment for the determination of mechanical properties and microstructural analysis. The mechanical tests conducted in this research included the tensile strength and hardness of the welded samples. Experiment with the 20 trials was conducted and the results were recorded. A minimum of three samples were considered for each trial and the average values recorded for respective responses.

3.5 Material Testing

Material testing as well as microstructural characterization were carried out on the welded samples and the base material (as-received) in order to obtain the microstructural changes and the properties of the weldments.

3.5.1 Tensile test

Tensile test also known as tension test is one of the most fundamental and common types of mechanical testing. In this study, three tensile specimens were cut from each of the welded samples as shown in Figure 3.3 and prepared to conform to the standard of the tensile machine used for the tensile testing.



Figure 3.3: Specimen for tensile test

The samples were subjected to tensile tests in accordance with ASTM E8 standard method. Each of the samples was mounted and gripped at both ends in a Hounsfield Tensometer, Type W with a capacity of 20 kN.The tensometer applies the force at a constant rate and

readings of force and extension were measured simultaneously by cell load and extensometer respectively, until the specimen finally breaks. The tensile strength is then calculated by taking the ratio of the breaking load and the cross-sectional area of the fractured sample.

3.5.2 Hardness test

Vickers Microhardness test method with a diamond indenter was used to performed the hardness test. The samples were first passed through metallographic sample preparation in order to obtain flat and smooth surface for regular indentation. Each of the prepared test samples were then placed on an anvil that has a screw thread base as shown in Figure 3.4. The indenter, which is in form of a right pyramid with a square base at an angle of 136^{o} between opposite faces was pressed into the fusion zone of the welded samples by a full load of 0.3kgf and it was applied for 10 to 15 seconds. The indentation was repeated along the lateral and transverse directions at 1.5 mm intervals in order to obtain the hardness profile of the welded samples. The two diagonals of the indentation left in the surface of the samples after removal of the load were measured using a microscope and their averages were calculated. The Vickers hardness, which is the quotient obtained by dividing the kgf load by the area (mm^2) of the indentation were then recorded directly from the computer interface attached to the machine.



Figure 3.4: Vickers microhardness testing machine

3.6 Microstructural Analysis

Microstructural examination was carried out on the welded samples and the base metal by using Optical Microscope (OPM) to reveal the microstructural changes due to heat energy input. After welding, the samples for investigation were prepared in accordance with the standard of the microscopic machine. The samples were first mounted in moulds with epoxy resin for easy handling prior to grinding and polishing operation. The mounted samples were then passed through grinding operation using different grit papers, starting from the rough (220 grit) to the finer grit (1200 grit) so that all scratches from cutting/sectioning were removed. During the grinding process, the direction of the samples was changed at right angle when moving from the previous grit to the next finer grit paper. This is to eliminate all the scratches produced from the previous grit papers and also, maintain the microstructural integrity of the specimen. The samples were then polished using a rotating polishing machine covered with a compound of alumina as the polishing

cloth. The samples were moved around the rotating wheel until a mirror-like surface was achieved for each of the samples. Finally, they were etched in 50% Acetic-Nital to reveal the microstructure. The setup was then loaded into the column of the microscopic machine which was connected to the monitor in a closed loop for which control and feedback were actualized.

CHAPTER FOUR

RESULTS AND DISCUSSION

This chapter provides the results obtained in the present investigation. The analysis of the results as well as the discussion were presented. The microstructures and mechanical properties of the weldment were also discussed. Table 4.1 presents the results of the experiment conducted. The experimental runs were carried out based on the designed matrix previously presented in Table 3.3. Both the results of the hardness and tensile strength obtained were given in the response column 5 and 6 of Table 4.1.

Experimental Run	Factors			Responses	
	A: Welding Current (A)	B: Welding Speed (mm/s)	C: Argon Flow Rate (L/min)	Tensile Strength (MPa)	Hardness (HV)
1	15	3	10	253	268
2	20	4	8	360	321
3	20	4	8	364	315
4	15	5	10	401	283
5	15	3	6	294	233
6	25	3	10	264	270
7	20	4	8	367	305
8	20	6	8	400	320
9	10	4	8	200	210
10	25	3	6	384	315
11	20	4	12	356	300
12	20	2	8	340	262
13	20	4	8	370	328
14	30	4	8	364	266
15	15	5	6	250	305
16	25	5	6	391	347
17	20	4	8	342	340
18	25	5	10	431	300
19	20	4	8	344	290
20	20	4	4	348	327

Table 4.1: Design matrix and responses for TIG welding process

4.1 Modeling for Tensile Strength

The modeling of tensile strength for FSS weld was performed using Design Expert version 10.0 software, by analyzing each of the response through the model tools including; Fit-Summary, Analysis of variance (ANOVA), Model diagnostics and model graphs (3-D surface and contour plot).

4.1.1 Fit summary statistics for tensile strength

The result of the fit summary statistic was presented in Table 4.2. The highest order polynomial with significant term for the tensile strength has F-value of 12.87 at $P \leq 0.0009$ as shown in the Table, and as such, quadratic is suggested.

Source	Sum of Squares	df	Mean Square	F Value	P-value Prob > F	
Mean vs Total	2.327E+006	1	2.327E+006			
Linear vs Mean	32504.46	3	10834.82	5.05	0.0119	
2FI vs Linear	20714.87	3	6904.96	6.58	0.0061	
Quadratic	**10832.00**	**3**	**3610.67**	**12.87**	**0.0009**	**Suggested**
Cubic vs Quadratic	1883.15	4	470.79	3.06	0.1072	Aliased
Residual	923.01	6	153.83			
Total	2.394E+006	20	1.197E+005			

Table 4.2: Fit Summary statistics for Tensile strength

4.1.2 Analysis of variance (ANOVA) test results for tensile strength

The analysis of variance for the tensile strength is presented in Table 4.3. The analysis was carried out at 5% significance level or 95% confidence level. It can be observed from the Table that the model is significant, having a p-value less than 0.05. Also, the lack of fit for

the model is greater than 0.05 which means, it is not significant which is desirable.There is a 14.76% chance that a "Lack of Fit F-value," this large, could occur due to noise. Equation 4.1 and 4.2 represent the model equation to predict the ultimate tensile strength (UTS) based on the process parameter variable with significant model terms (A, B, AC, BC and A^2) as shown in Table 4.3. The model equations were developed from the improved analysis of variance by removing all the model with insignificant terms. Equation 4.1 identifies the relative impact of each parameter on the ultimate tensile strength based on the coefficient of each of the variable. From the equation, it can be observed that the most influential parameter on the tensile strength is the welding current with the highest coefficient, followed by welding speed and the least significant factor is the argon flow rate.

Equation 4.2 can be used to make predictions about the response for given levels of each factor. However, the equation cannot be used to determine the relative impact of each factor because the coefficients are scaled to accommodate the units of each factor and the intercept is not at the center of the design space.

Table 4.3: Analysis of variance (ANOVA Table) for the tensile strength

Source	***Sum of Squares***	***df***	***Mean Square***	***F Value***	***P-value Prob > F***	
Model	*63119.19*	*6*	*10519.87*	*36.58*	*< 0.0001*	***significant***
A-Current	*22477.51*	*1*	*22477.51*	*78.17*	*< 0.0001*	
B-Speed	*9895.28*	*1*	*9895.28*	*34.41*	*< 0.0001*	
C-Argon flow rate	*131.68*	*1*	*131.68*	*0.46*	*0.5105*	
AC	*4564.90*	*1*	*4564.90*	*15.87*	*0.0016*	
BC	*15549.66*	*1*	*15549.66*	*54.07*	*< 0.0001*	
A^2	*10500.17*	*1*	*10500.17*	*36.51*	*< 0.0001*	
Residual	*3738.30*	*13*	*287.56*			
Lack of Fit	*3028.09*	*8*	*378.51*	*2.66*	*0.1476*	***not significant***
Pure Error	*710.21*	*5*	*142.04*			
Cor Total	*66857.49*	*19*				

a. Model Equation in terms of coded factor for the tensile strength

$$UTS = +356.84 + 37.48A + 24.87B + 2.87C - 23.89AC + 44.09BC - 19.65A^2 \quad 4.1$$

b. Model Equation in terms of actual factors for the tensile strength

UTS = +104.79853 + 58.04272 x current -151.48125 x speed – 38.96563 x argon flow rate – 2.3888 x current x argon flow rate + 22.0438 x speed x argon flow rate – 0.78591x current 4.2

4.1.3 Model adequacy test and validation for tensile strength

The model adequacy is analytically verified by assessing the following model tool as presented in Figure 4.1 – 4.5. These model tools which include; the perturbation plot (Figure 4.1) the normal plot of residual (Figure 4.2), residual plot versus predicted value (Figure 4.3), residual versus run (Figure 4.4) and the Box-cox plot for power transformation shown in Figure 4.5.

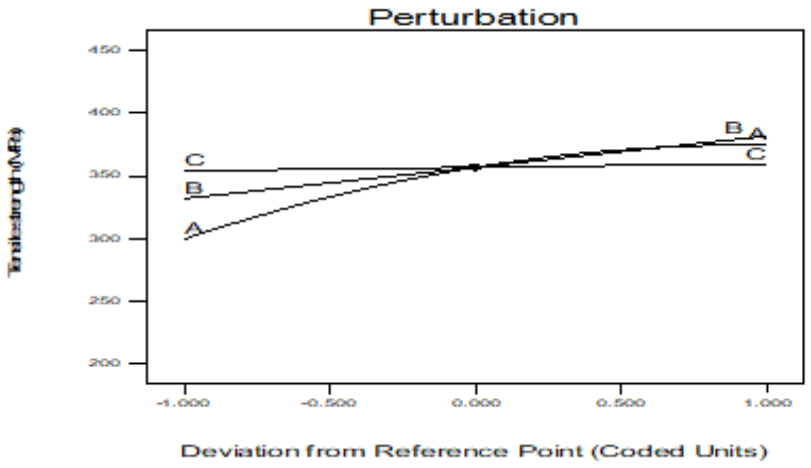


Figure 4.1:Perturbation plot for tensile strength

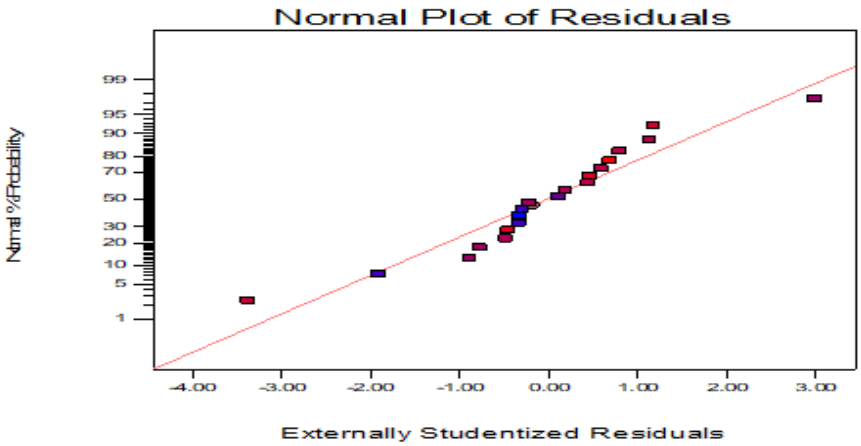


Figure 4.2: Normal probability plot of residuals for tensile strength

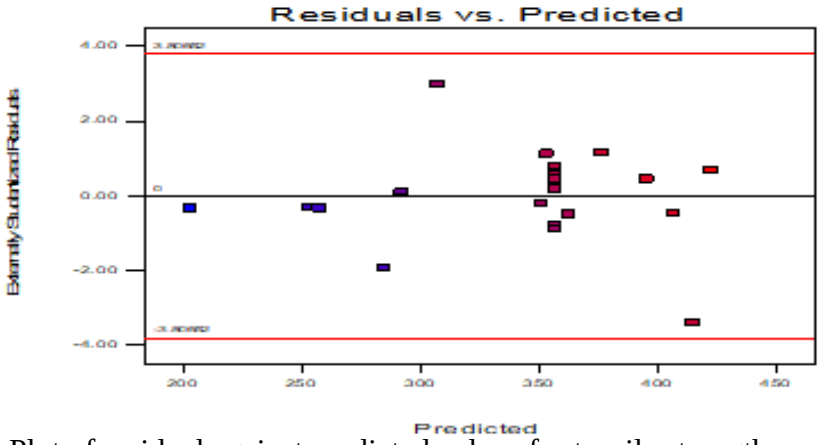


Figure 4.3:Plot of residual against predicted values for tensile strength

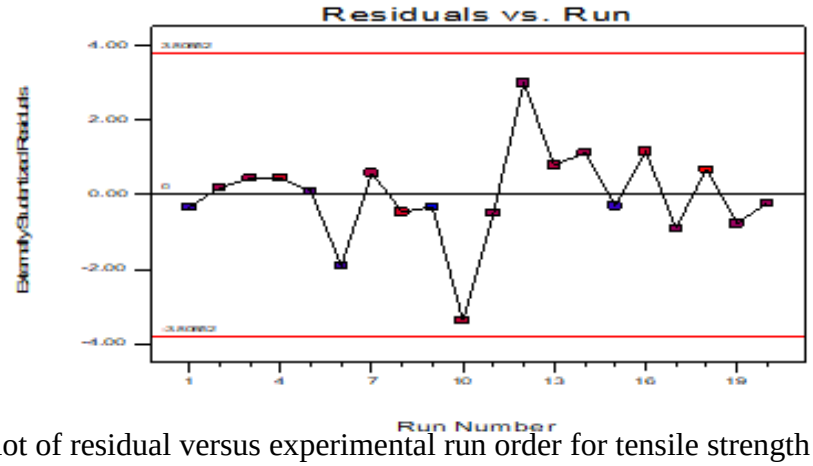


Figure 4.4:Plot of residual versus experimental run order for tensile strength

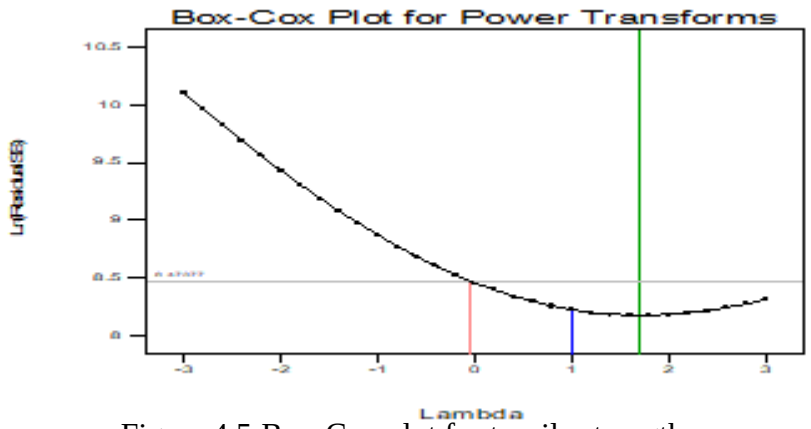


Figure 4.5:Box-Cox plot for tensile strength

Table 4.4 presents the statistical summary which shows the amount of variability of the mean data. From the Table, the predicted R^2 of 0.8327 is in reasonable range of acceptance since the difference with the adjusted R^2 (0.9183) is less than 0.2. Also, the adequate precision of 21.862 which measures the signal to noise ratio also indicates an adequate signal which implies that the model can be used to navigate the design space since it is well above the required value of 4.0 as suggested by the design expert.

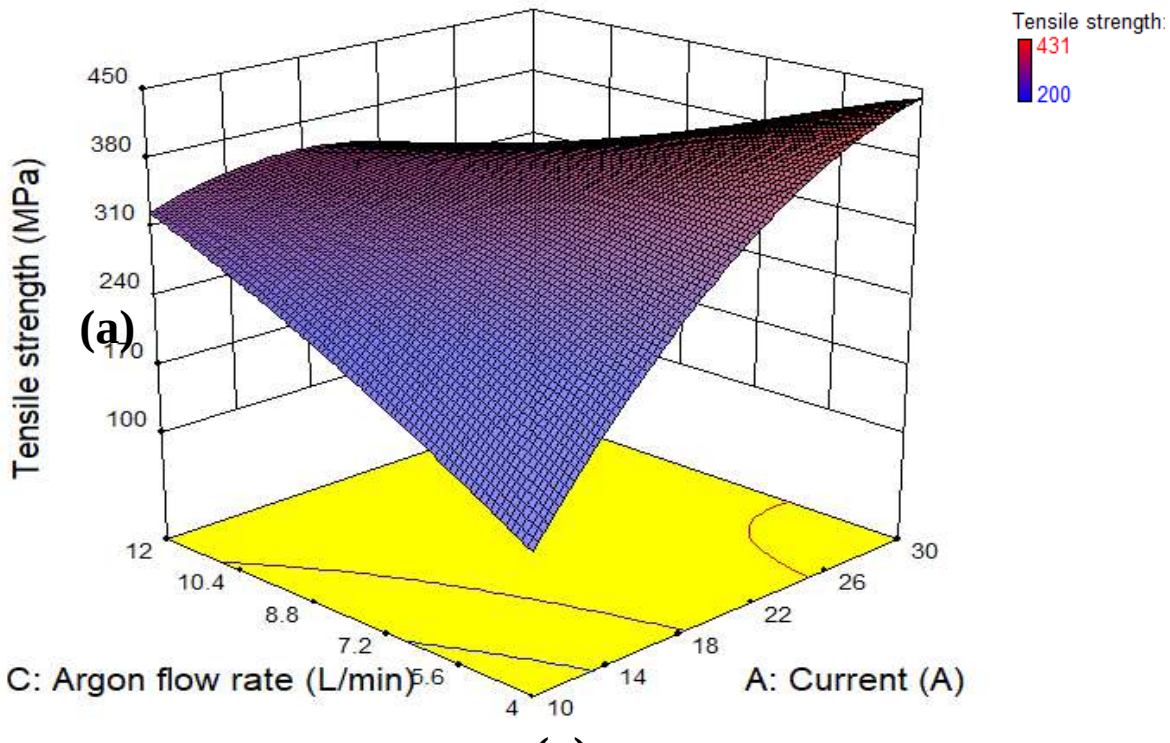
Standard deviation	16.96	R-Squared	0.9441
Mean	341.12	Adjusted R Squared	0.9183
Coefficient of variation	4.97	Predicted R-Squared	0.8327
		Adequate Precision	21.862

Table 4.4: Summary of model statistics for Tensile Strength

4.1.4 Surface and contour plot for tensile strength

The 3-D surface graphs and contour plots for the tensile strength are presented in figures 4.6 - 4.8. For the surface plots the input variables are shown in x and y axes while the response is presented on the z axis, which ultimately reveal the optimal level. The graph shown in Figure 4.6 (a) and (b) represents the effect of the interaction between two factors (current and argon flow rate) on the response (tensile strength). Figure 4.7 presents the

effect of the interaction between the current and speed on the tensile strength. While Figure 4.8 shows the interactions between the speed and the gas flow rate on the tensile strength.



(a)

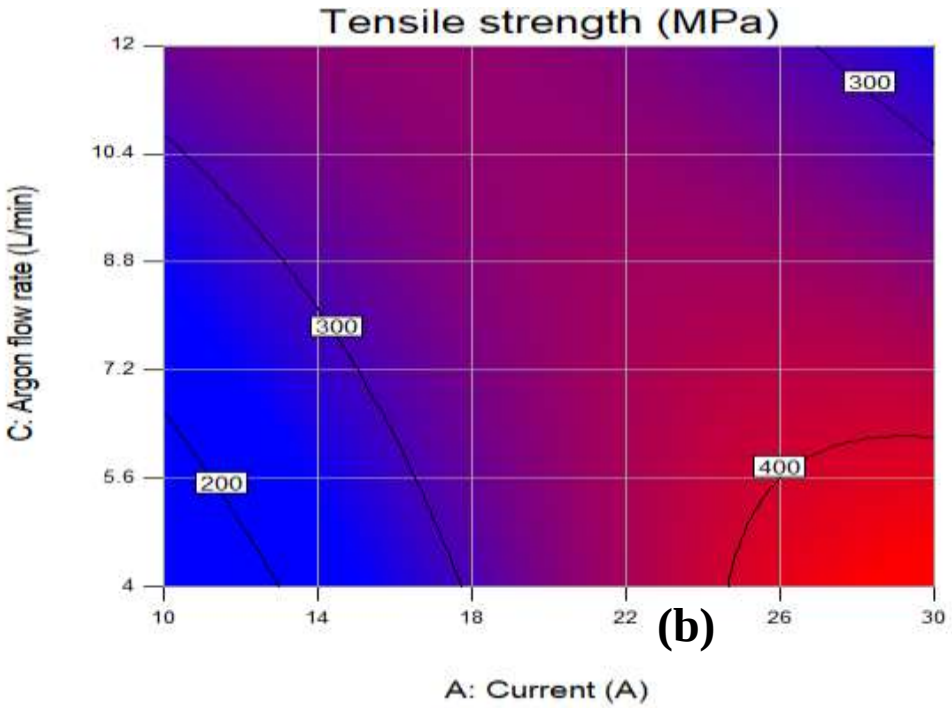
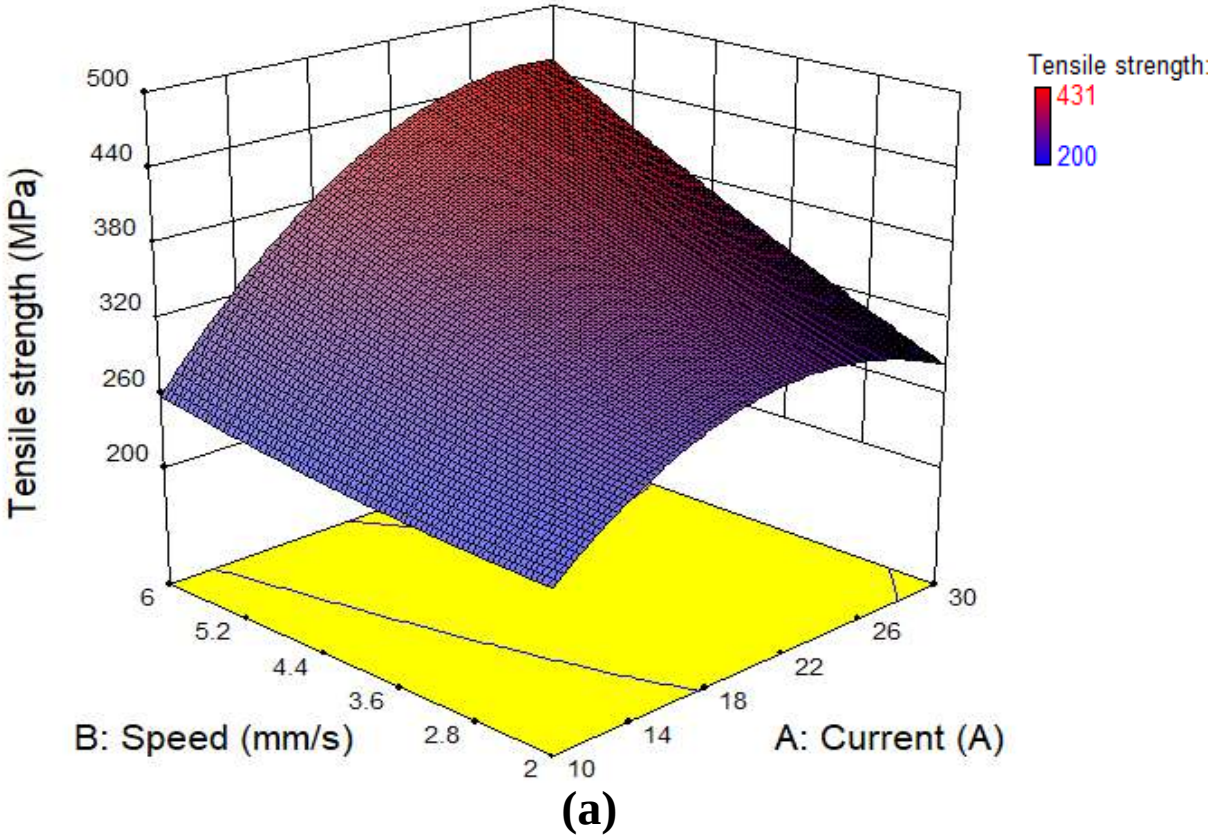


Figure 4.6: Surface and contour plot showing the variation of tensile strength with welding current and gas flow rate (a) 3-D surface plot (b) Contour plot



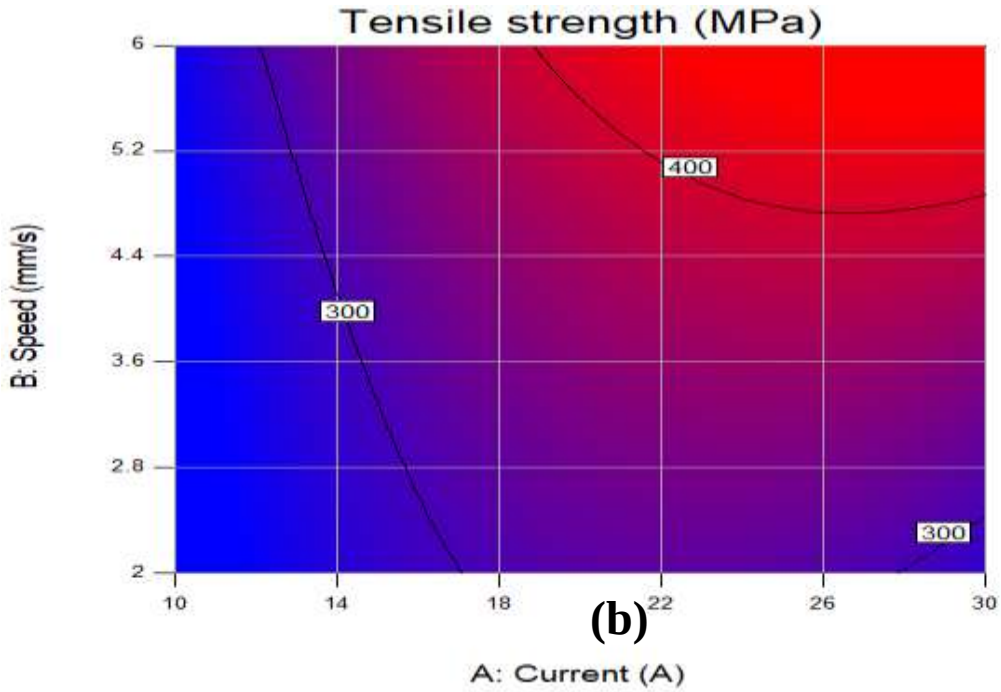
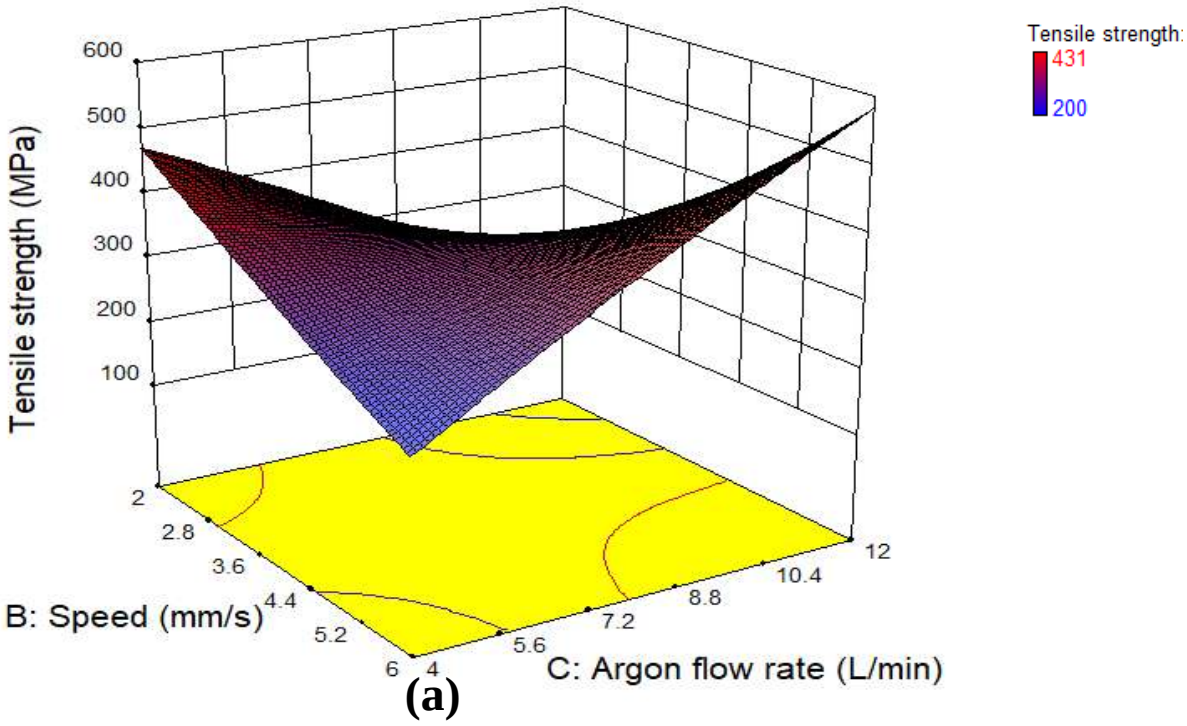


Figure 4.7: Surface and contour plot showing the variation of tensile strength with welding current and welding speed (a) 3-D surface plot (b) Contour plot.



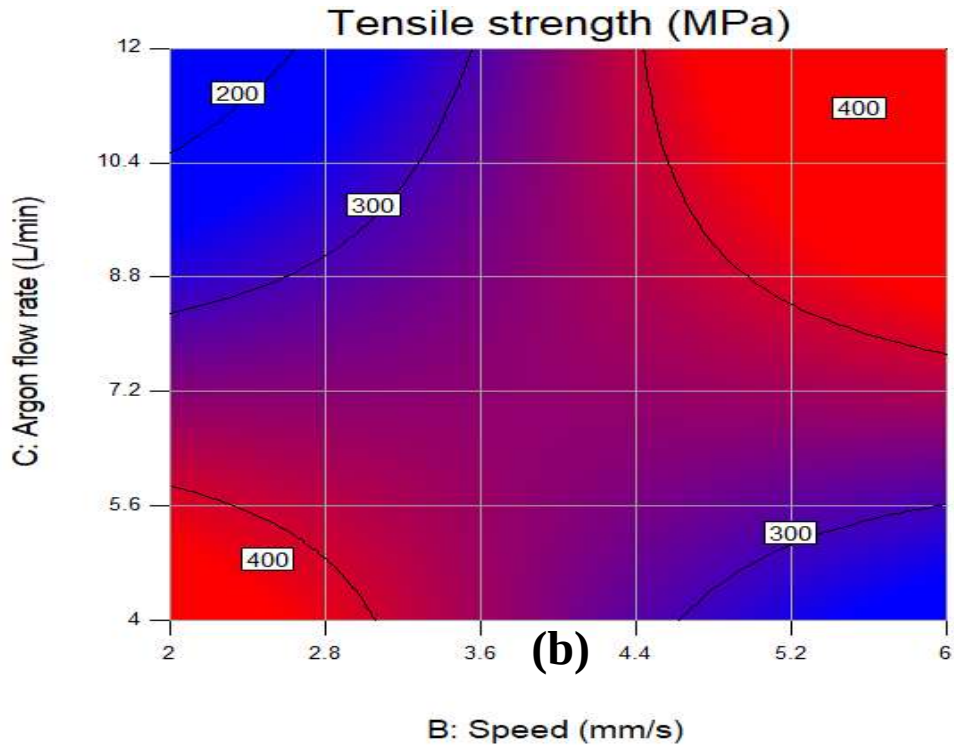


Figure 4.8: Surface and contour plot showing the variation of tensile strength with welding speed and the argon flow rate (a) 3-D surface plot (b) Contour plot.

4.1.5 Discussion

The perturbation plot shown in Figure 4.1 represents the effects of each of the process parameters on the tensile strength. From the plot, it was observed that current has the greatest influence on the tensile strength which increases gradually from the reference point to a maximum and decreases at higher current confirming quadratic effect of current on the response as also indicated in Table 4.2. The argon flow rate is almost linear which indicates that it has little significance on the tensile strength.

The normal probability plot of the residuals for tensile strength shown in Figure 4.2 reveals that the residuals (errors) are falling on the straight line, which means the errors are distributed normally. This clearly indicates an excellent adequacy of the regression model based on the RSM design expert.

Figure 4.3 shows the plot of residual versus predicted values for the tensile strength and it can be seen that the data did not follow any definite pattern but are within the accepted limit, hence, the data is considered to be adequate to predict the tensile strength.

Figure 4.4 presents the plot of residual against the run order which also satisfy the adequacy requirement of the model by showing a randomly scattered values without any relationship towards either of the two ends, indicating the adequacy of the model.

The last model tool used to assess the adequacy of the developed model is the Box-Cox transformation shown in Figure 4.5. It was observed from the Figure that the value of λ (confidence level) is unity, therefore, no transformation is recommended. Hence, it can be concluded that the normality and residual displayed from the Box-Cox plot are adequate to predict the tensile strength.

From Figure 4.6, the tensile strength is minimum at a current of 10A and argon flow rate of 4L/min. It increases gradually with increase in the current with little rise in the flow rate and peak at about 26A. As the flow rate is further increased to 12L/min, the tensile strength reduces even though there are no significant changes in the current. This clearly showed that the interaction between the current and the gas flow rate has effect on the tensile strength of the weldment. However, the effect of the gas flow rate is minimal compared with that of the current. The trend displayed by the tensile strength in Figure 4.7 is different from Figure 4.6, as the tensile strength increases with increase in both current and the welding speed. Maximum value of tensile strength was achieved at a current of 25A and speed of 5mm/s. As the current increases further to 30A and at a speed of about 3mm/s, there is a decrease in the tensile strength. This trend of result is similar to the study conducted by Subhas, *et al*. (2019). The decrease in the tensile strength at higher current and lower speed may be due to high heat energy input into the welded joint which may induces coarse grains in the weld and heat affected zone, thereby reducing the properties of

the weldment (Subhas, *et al*. (2018). From Figure 4.8, the tensile strength is minimal at a flow rate of 12L/min and a speed of 2mm/s, it then increases gradually as the gas flow rate decrease while the speed remains constant at 2mm/s. Similarly, the tensile strength also peaks at higher speed of 6mm/s and at a flow rate of 12L/min. These results confirm the significant interaction between the speed and the flow rate as shown in the ANOVA Table 4.4.

4.2 Modeling for Hardness

The model development was performed using Design Expert version 10 software, by analyzing each of the response through the model tools including; Fit-Summary, Analysis of variance (ANOVA), Model diagnostics and model graphs (3-D surface and contour plot).

4.2.1 Fit summary statistics for hardness

The highest order polynomial with significant term for the hardness has F-value of 15.01 at $P \leq 0.0005$ as presented in Table 4.5 and the highest order of polynomial suggested by the model is the quadratic as indicated in the Table.

Source	Sum of Squares	df	Mean Square	F Value	P-value Prob >F	
Mean vs Total	1.755E+006	1	1.755E+006			
Linear vs Mean	11378.63	3	3792.88	4.04	0.0257	
2FI vs Linear	2772.78	3	924.26	0.98	0.4315	
Quadratic	**10015.78**	**3**	**3338.59**	**15.01**	**0.0005**	**Suggested**
Cubic vs Quadratic	649.12	4	162.28	0.62	0.6660	Aliased
Residual	1574.73	6	262.46			
Total	1.781E+006	20	89048.96			

Table 4.5: Fit Summary statistics for Hardness

4.2.2 Analysis of variance (ANOVA) test results for hardness

The analysis of variance for the hardness with all the model terms is presented in Table 4.6. The model is significant having a p-value less than 0.05. Equation 4.3 and 4.4 represent the model equation to predict the hardness (Hr) based on the process parameter variable with significant model terms (A, B, AC, B^2 and A^2) as shown in the Table 4.6. The model equations were developed from the analysis of variance. Equation 4.3 identifies the relative impact of each parameter on the hardness based on the coefficient of each of the variable. From the equation, it can be observed that the most influential parameter on the hardness in the order of importance is the welding speed, welding current, and the argon flow rate. Equation 4.4 can be used to make predictions about the response for given levels of each factors.

Table 4.6: Analysis of Variance (ANOVA Table) for Hardness

Source	Sum of Squares	df	Mean Square	F Value	P-value Prob > F	
Model	*24157.37*	*7*	*3451.05*	*18.54*	*< 0.0001*	***significant***
A-Current	*4715.23*	*1*	*4715.23*	*25.33*	*0.0003*	
B-Speed	*5177.88*	*1*	*5177.88*	*27.82*	*0.0002*	
C-Argon flow rate	*1485.52*	*1*	*1485.52*	*7.98*	*0.0153*	
AC	*1994.91*	*1*	*1994.91*	*10.72*	*0.0067*	
BC	*773.62*	*1*	*773.62*	*4.16*	*0.0641*	
A^2	*9823.66*	*1*	*9823.66*	*52.78*	*< 0.0001*	
B^2	*956.97*	*1*	*956.97*	*5.14*	*0.0426*	
Residual	*2233.67*	*12*	*186.14*			
Lack of Fit	*697.12*	*7*	*99.59*	*0.32*	*0.9130*	***not significant***
Pure Error	*1536.55*	*5*	*307.31*			

Cor Total	*26391.05*	*19*

a. Model Equation in terms of coded factor for the Hardness

$$Hardness = +316.46 +17.17A +17.99B -9.64C -15.79AC -9.83BC -19.31A^2 -6.03B^2 \quad 4.3$$

b. Model Equation in terms of actual factors for the Hardness

$$Hardness = -600.95857 + 46.95809x\ Current + 105.53295x\ Speed + 46.43219x\ Argon\ flow\ rate -1.57913x\ Current\ x\ Argon\ flow\ rate - 4.91688\ x\ Speed\ x\ Argon\ flow\ rate- 0.77229\ x\ Current^2 - 6.02607x\ Speed^2 \quad 4.4$$

4.2.3 Model adequacy test and validation for hardness

The tools used to verify adequacy of the model on the hardness are presented in Figures 4.9 – 4.13. Figure 4.9 shows the perturbation plot for the hardness while the normal probability plot of residual is presented in Figure 4.10.

Figure 4.11 shows the plot of residual versus predicted values for the hardness. Figure 4.12 presents the plot of residual against the run order, while Figure 4.13 shows the Box-Cox power transformation curve for the hardness of the weldment.

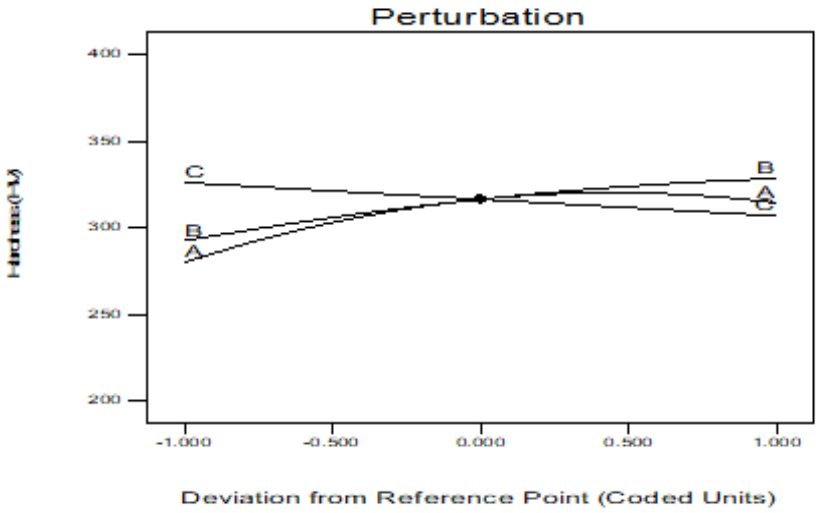


Figure 4.9:Perturbation plot for hardness

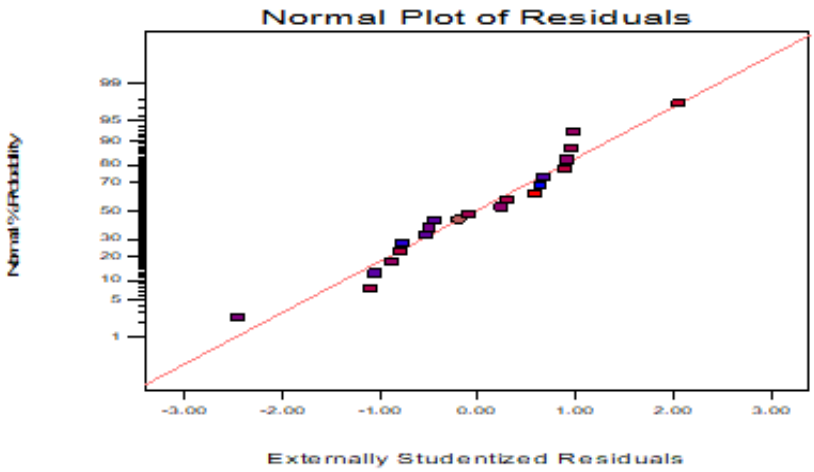


Figure 4.10:Normal probability plot of residuals for the hardness

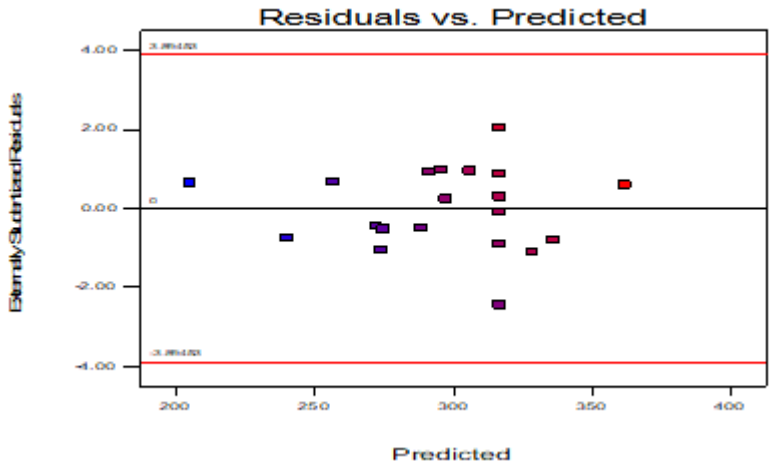


Figure 4.11:Plot of residual against predicted values for hardness

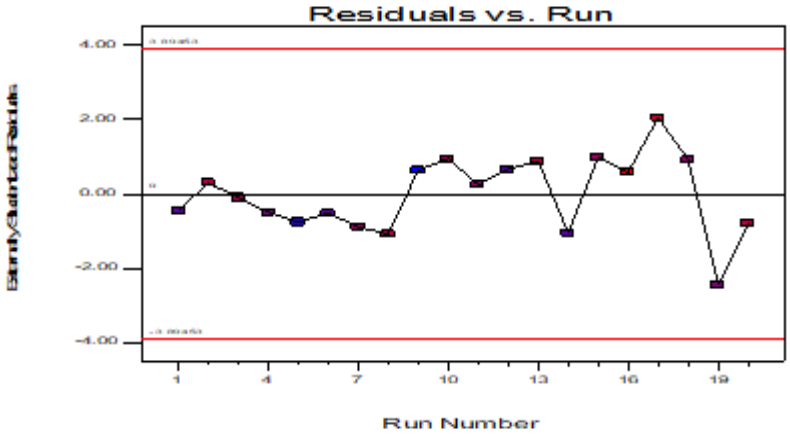


Figure 4.12:Plot of residual versus experimental run order for hardness

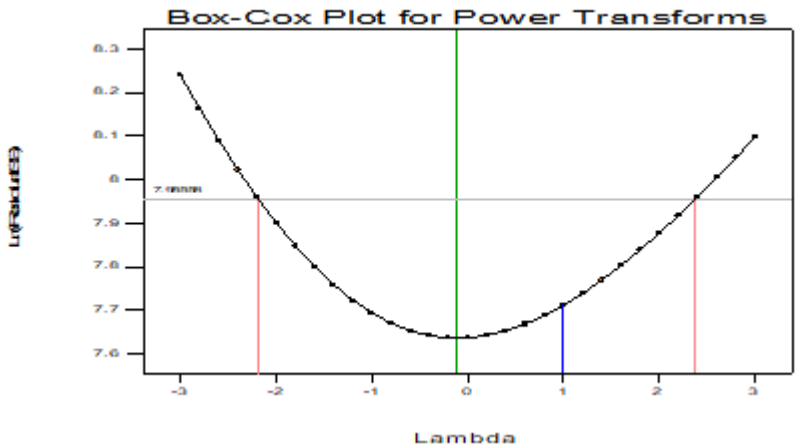


Figure 4.13:Box-Cox plot for hardness

The statistical summary presented in Table 4.7 is used to explain the amount of variability of the mean data. From the Table, the predicted R^2 of 0.7878 is in reasonable range of acceptance since the difference with the adjusted R^2 (0.8660) is less than 0.2. Also, the adequate precision of 18.154 which measures the signal to noise ratio also indicates an adequate signal which implies that the model can be used to navigate the design space since it is well above the required value of 4.0 suggested by the design expert.

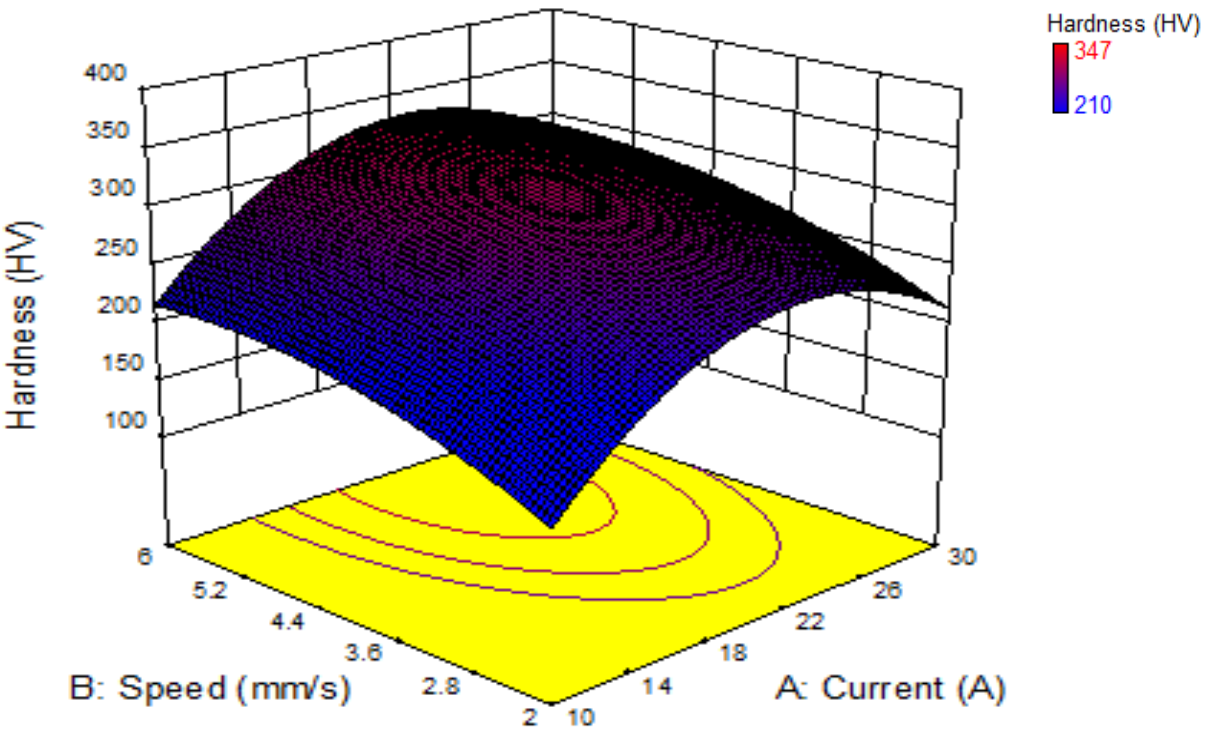
Table 4.7: Summary of model statistics for hardness

Standard deviation	13.64	R-Squared	0.9154
Mean	296.19	Adjusted R-Squared	0.8660
Coefficient of variation	4.61	Predicted R-Squared	0.7878
		Adequate Precision	18.154

4.2.4 Surface and contour plot for hardness

The 3-D surface graphs and contour plots for the hardness are presented in Figures 4.14 - 4.16. Both the 3-D and the contour plots explain the effects of interactions between the variables on the hardness of the weldment. The graph shown in Figure 4.14 (a) and (b) represents the effect of the interaction between the current and the speed on the hardness. Figure 4.15 (a) and (b) showed the influence of both current and the gas flow rate on the hardness property. It can also be observed from the graphs that the two input variables have positive effects on the hardness value of the welds. While the surface and the contour

plot in Figure 4.16 (a) and (b) respectively show the effects of interactions between the welding speed and the argon flow rate on the hardness value of the weldment.



(a)

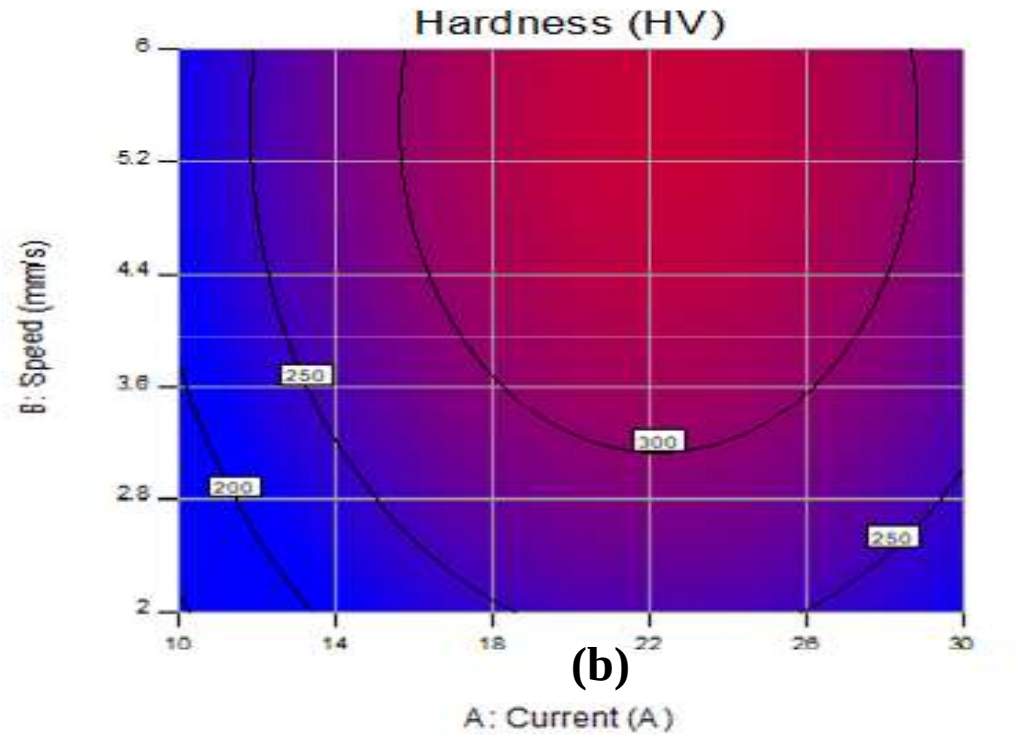
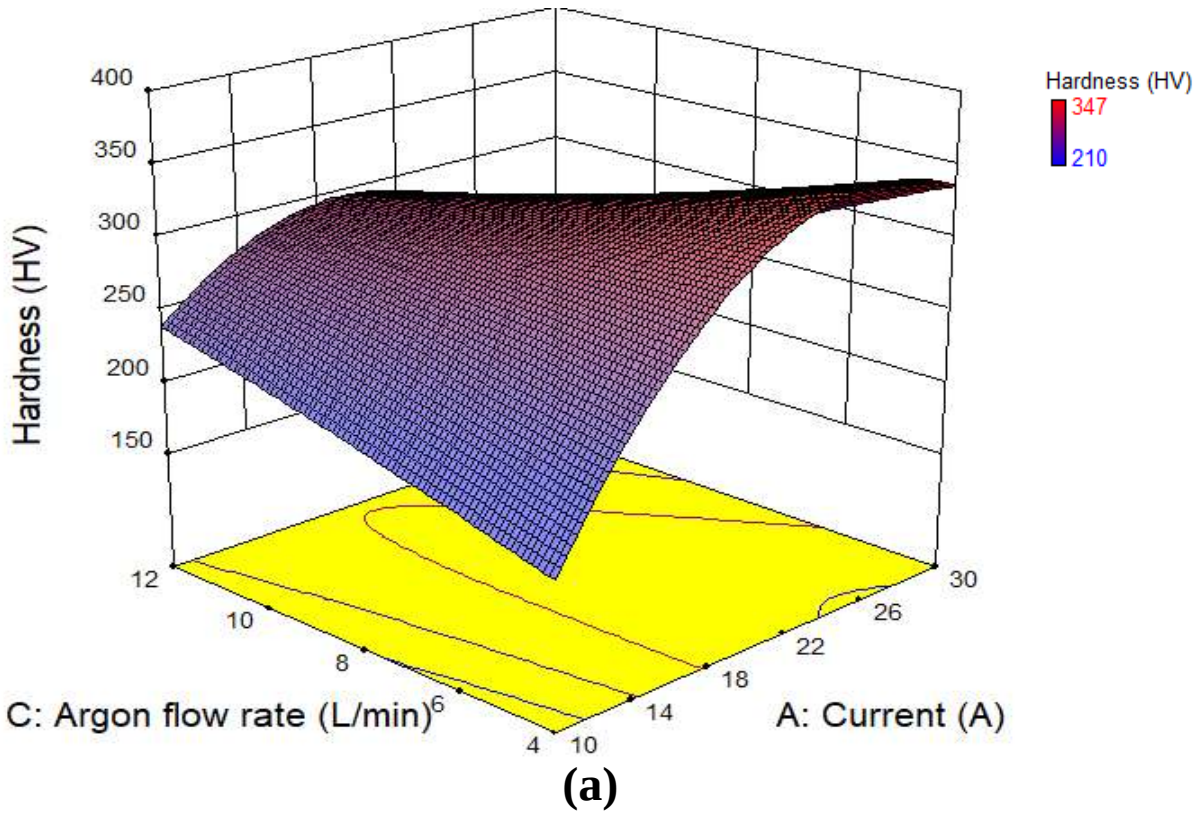


Figure 4.14: Surface and contour plot showing the variation of hardness with welding current and speed (a) 3-D surface plot (b) Contour plot.



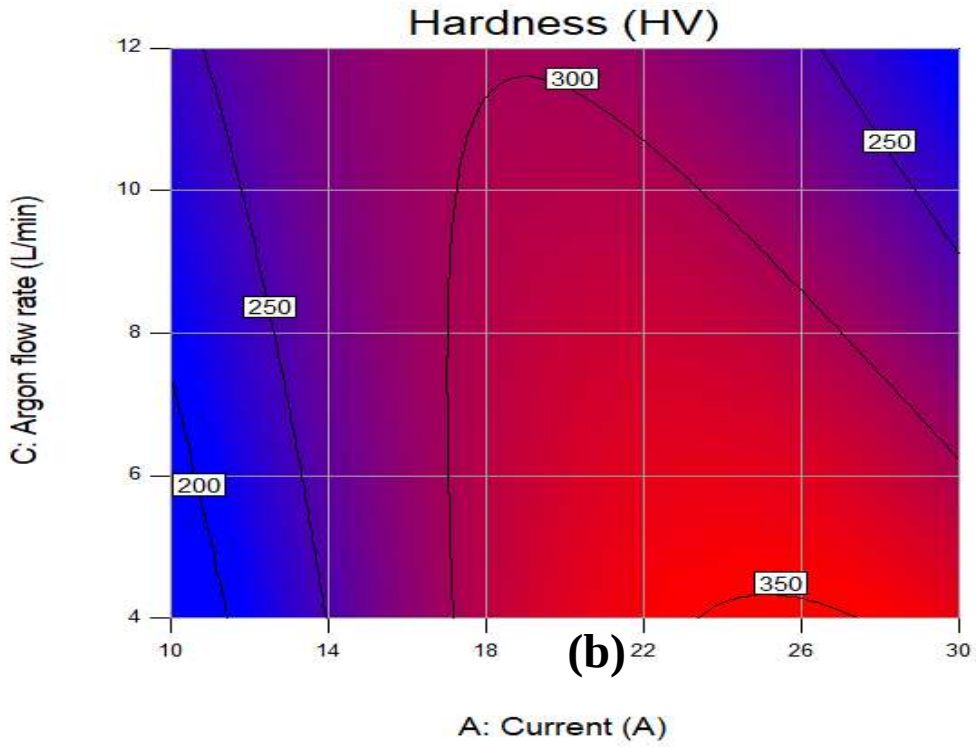
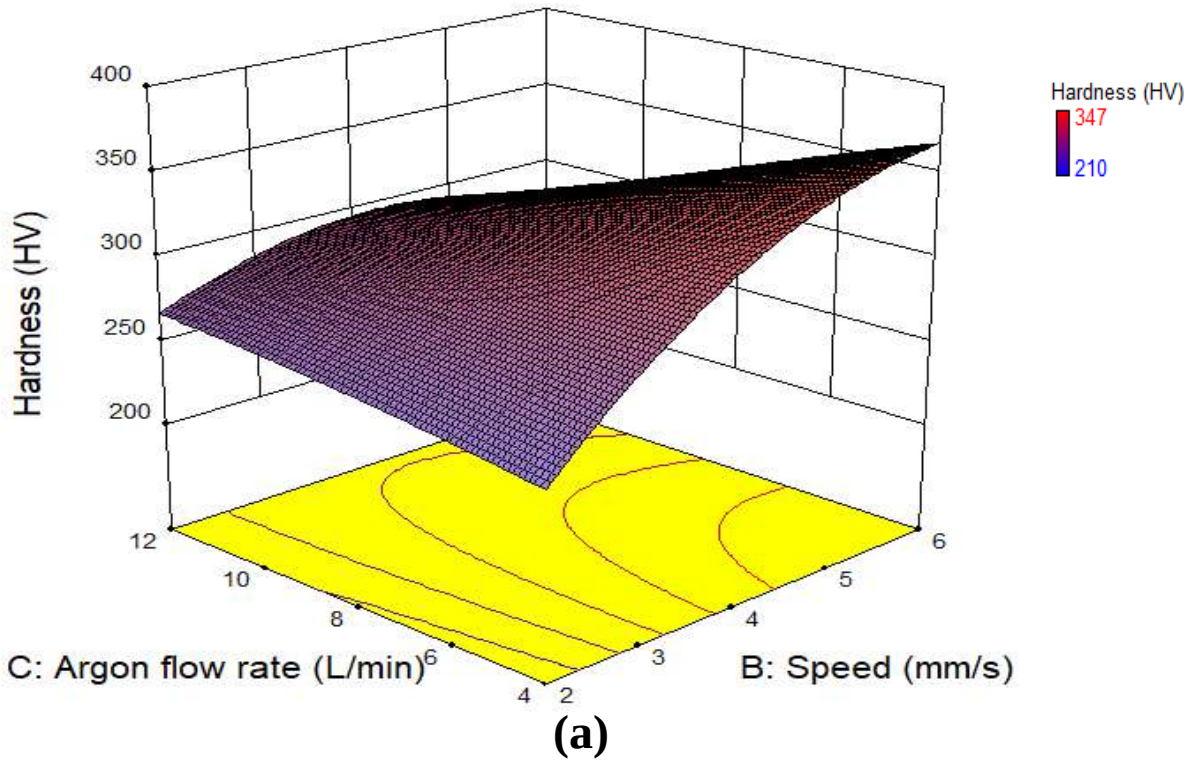


Figure 4.15: Surface and contour plot showing the variation of hardness with welding current and the argon flow rate (a) 3-D surface plot (b) Contour plot.



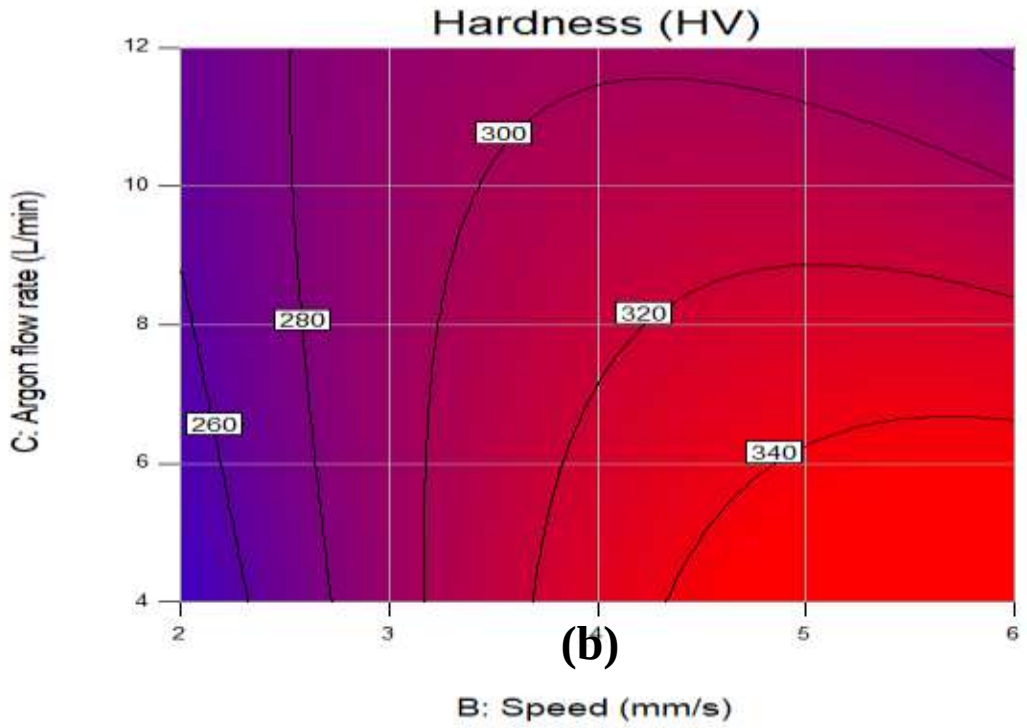


Figure 4.16: Surface and contour plot showing the variation of hardness with welding speed and the argon flow rate (a) 3-D surface plot (b) Contour plot.

4.2.5 Discussion

The perturbation plot shown in Figure 4.9 represents the effects of each of the process parameters on the hardness. From the plot, it can be seen that current and speed have almost similar influence on the hardness property which also increases gradually from the reference point to a maximum value and decrease at higher current and speed confirming the quadratic effect of the variables on the hardness. Again, the argon flow rate is almost linear which indicates that it has little significance on the hardness.

The normal probability plot of the residuals for hardness shown in Figure 4.10 also reveals that the residuals (errors) are falling on the straight line, hence, indicating the normal distribution of the errors. This clearly shows an excellent adequacy of the regression model based on the RSM design expert.

Figure 4.11 showed that the data did not follow any definite pattern but, are within the accepted limit, hence, the data is considered to be adequate to predict the hardness property of the weldment.

Figure 4.12 satisfies the adequacy requirement of the model by showing a randomly scattered values without any relationship towards either of the two ends, indicating the adequacy of the model. From the transformation curve shown in Figure 4.13, it is observed that the value of λ (confidence level) is unity, no transformation is recommended to the model. Hence, it can be concluded that Box-Cox plot are adequate to predict the hardness property.

From the 3-D surface and the contour plots shown in Figure 4.14, it can be observed that hardness increases with increase in both the current and speed to about 330HV and begin to drop as the current increases further above 25A and speed above 5mm/s. The hardness is minimum at a current of 10A and a speed of 3mm/s. The decrease in the hardness at lower current and speed was due to lack of proper weld penetration at lower current and speed. Hence, the interaction between current and the speed significantlyinfluences the hardness of the weld (Navaneeswar and Venkata, 2018).

From Figure 4.15, The hardness increases gradually from 200HV to about 350HV at a current of 26A and a gas flow rate of about 5L/min. However, as the current and the flow rate further increases to 30A and 12L/min respectively, the hardness dropped to about 250HV as shown in Figure 4.15(b), this may be attributed to high heat energy input to the weld joint causing increase in the grain size, hence, reduces the hardness of the weldment (Amuda and Mridha, 2010).

It is clearly observed from Figure 4.16 that the hardness value increases with increase in the welding speed and decreases with increase in the argon flow rate as shown by the blue and the red portion indicating higher and lower hardness value respectively. Maximum

hardness of about 360HV was obtained at a speed of 6mm/s and gas flow rate of 4L/min. As the gas flow rate increases to about 11L/min and the speed is reduced to 4mm/s, the hardness reduces to 304HV as indicated in Figure 4.16 (b). This variation is due to the fact that; higher welding speed usually requires high current in order to achieve the require penetration in the weld joint. However, if the gas flow rate is very high at high welding current, there may be too much oxidation at the welding zone which may reduce the hardness property of the weldment (Sharmistha and Neha, 2016).

4.3 Multi-Objective Optimization (*MOO*) for Response Performance

The response surface models generated for the tensile strength and hardness have been described in section 4.1 and 4.2 respectively. The analysis indicates that, both models can sufficiently be used in generating their points of desirable results within the design conditions since the desirable process condition for one response was different from the other response. The optimization condition for this work are presented in Table 4.8.

Table 4.8: Optimization condition for the process parameter and responses

Name	**Goal**	**Lower Limit**	**Upper limit**
A: Current (A)	is in range	15	25
B: Speed (mm/s)	is in range	3	5
C: Argon flow rate (L/min)	is in range	6	10
Tensile strength (MPa)	maximize	200	431
Hardness (HV)	maximize	210	347

Table 4.9 presents the optimal performance for each of the responses investigated. Solution No 1 was selected as the optimum condition for the process with a maximum tensile strength and hardness of 431.014 MPa and 307.1 HV respectively with desirability of 1, which indicates that the two responses have close property relationship with that of the base material

Table 4.9: Optimal solution for the responses.

S/N	Current	Speed	Argon flow rate	Tensile strength	Hardness	Desirability	
1	**21.737**	**5.000**	**10.000**	**431.014**	**307.100**	**1.000**	**Selected**
2	21.681	5.000	10.000	431.013	307.231	1.000	
3	21.807	5.000	10.000	431.010	306.927	1.000	
4	21.844	5.000	10.000	431.004	306.833	1.000	
5	21.484	5.000	10.000	430.967	307.660	0.999	
6	21.767	5.000	9.995	430.917	307.091	0.999	
7	21.330	5.000	10.000	430.889	307.952	0.999	
8	22.163	5.000	10.000	430.867	305.933	0.999	
9	22.243	5.000	10.000	430.807	305.683	0.999	
10	21.187	5.000	10.000	430.783	308.191	0.999	
11	22.338	5.000	10.000	430.723	305.375	0.998	
12	22.440	5.000	10.000	430.618	305.027	0.998	
13	20.981	5.000	9.999	430.544	308.495	0.998	

4.3.1 Confirmatory test

In order to validate the test results of the optimization obtained from the developed model, confirmatory experiment was conducted using the predicted optimal conditions. The confirmatory test performed is presented in Table 4.10. The results observed from the experiment were then compared with the predicted values for the responses and the percentage errors were calculated. It can be observed that the predicted and observed results were in a good agreement with percentage errors of 1.23 and 1.81 for tensile strength and hardness respectively, which is within the satisfactory range of 10% error (Vidyarthy et al. 2017).

Process Parameter			Tensile Strength (MPa)			Hardness (HV)		
Current (A)	Speed (mm/s)	AFR (L/min)	Predicted	Experimented	% Error	Predicted	Experimented	% Error
21.737	5	10	431.014	425.705	1.23	307.10	301.532	1.81

Table 4.10: Confirmatory test result

4.4 Characteristics of Optimized TIG Ferritic Stainless Steel Weld

Table 4.11 presents the mechanical properties of both the base metal and the welded sample with optimized process parameters. Based on this result, it can be observed that the FSS weld has close properties with the base metal, indicating that it is less affected by the heat. Also, the result shows that all the welded samples have greater hardness values than the base metal with the optimum value of 307.1HV. This increase in hardness may be attributed to the formation of martensite structures at the fusion zones of the weld metal.

Material	**Tensile strength (MPa)**	**Hardness (HV)**	**% Elongation**
Base metal	446.7	263	38.8
Welded sample at optimized condition	431.014	307.10	28.3

Table 4.11: Mechanical properties of base metal and welded metal at optimized condition

4.4.1 Weld topography

The topographies of the weld tracks produced under different process parameter conditions are shown in Plate 4.1 (a-c). Heat energy input depends on the welding current and speed which appear to be the most prominent factors controlling the weld quality, therefore, the topographies of the weld metal assessed were selected based on the least and highest heat input corresponding to run no. 9 and 14 respectively, as well as weld with optimized heat input. The heat energy input was calculated using equation 2.2. The surface of the welds was captured with a high resolution 14MP Panasonic digital camera. It can be observed that the topography of the optimized weld (Plate 4.1 (c)) is smoother, continuous and defect free compared to welds at the two extreme heat energy inputs. Weld at very low heat input in Plate 4.1 (a) showed the existence of porosities along the weld track, while in Plate 4.1 (b), there is evidence of high heat energy into the weld joint with poor weld

surface quality

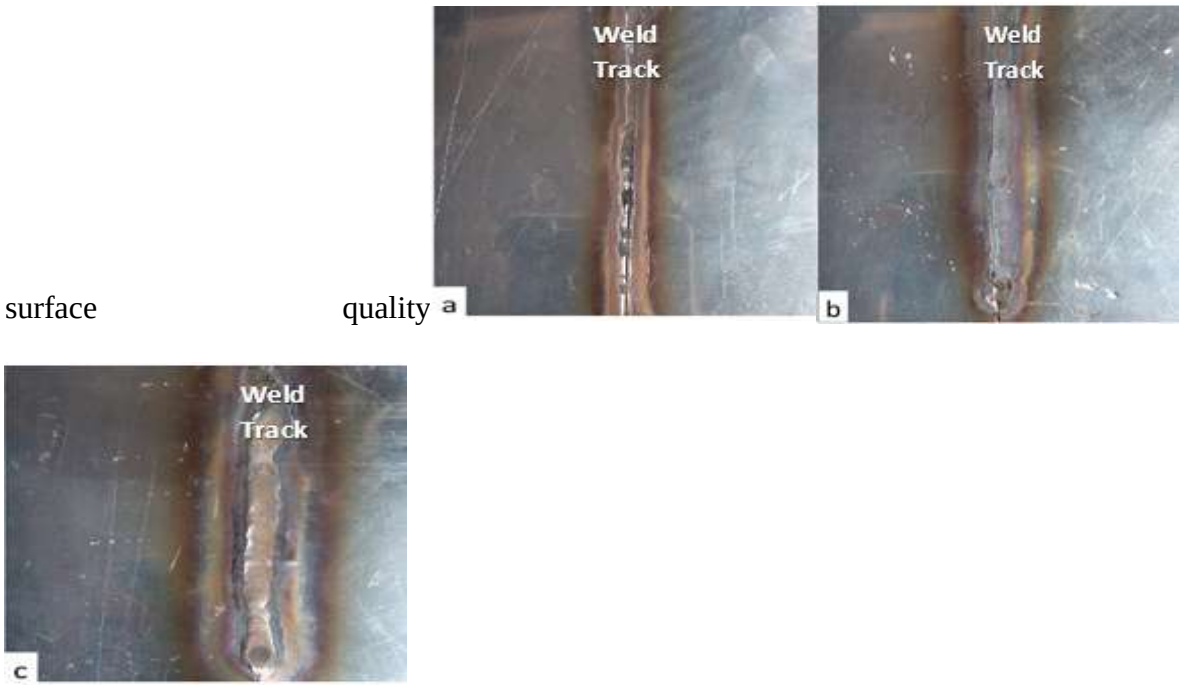


Plate 4.1: Topographies of the welds at different heat energy conditions: (a) 58 J/mm (b) 174 J/mm (c) 102 J/mm

4.4.2 Microstructural analysis

The optical micrographs of some of the selected samples were shown in Plate 4.2-4.7. The selection of these weld samples for the microstructural investigation is based on the responses with maximum, minimum and optimal mechanical properties. It was observed that the grain growth took place from the edge of the heat-affected zone (HAZ) to the fusion boundary in all the welded samples considered. However, the level of the grain coarseness depends on the condition of heat energy input applied.

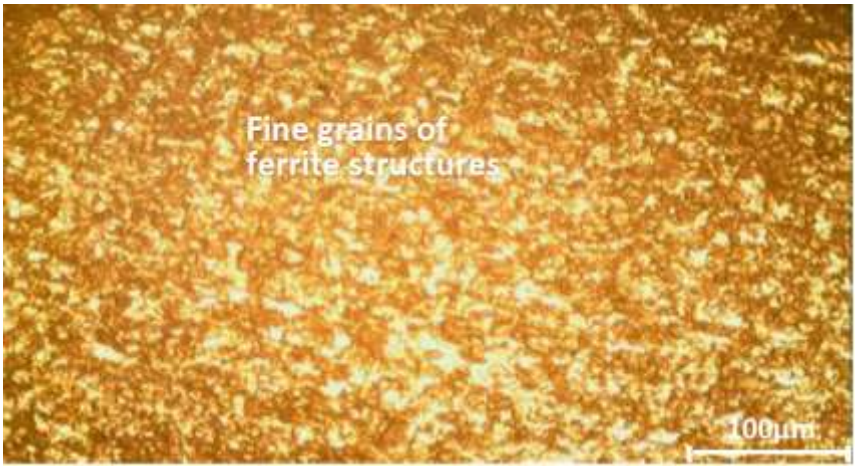


Plate 4.2: Micrograph of the base metal etched with 50% Acetic-Nital (x100)

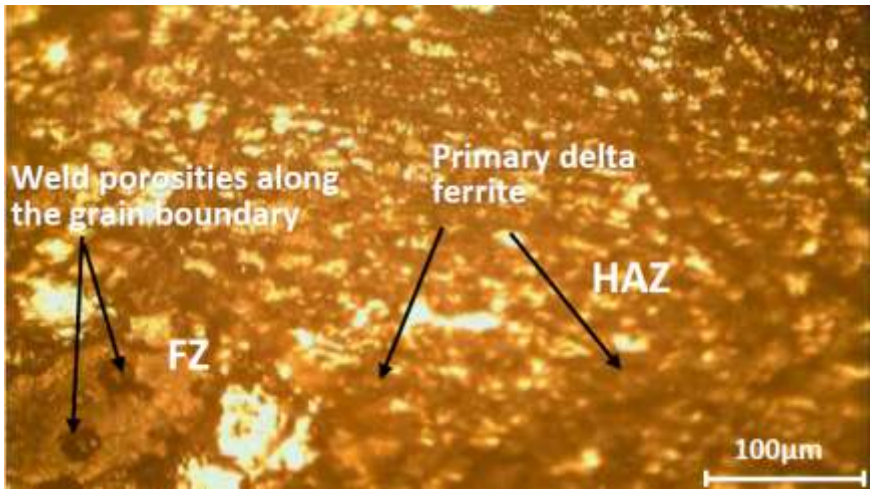


Plate 4.3: Micrograph of TIG welded ferritic stainless steel at 58J/mm (Run 9), etched with 50% Acetic-Nital (x100)

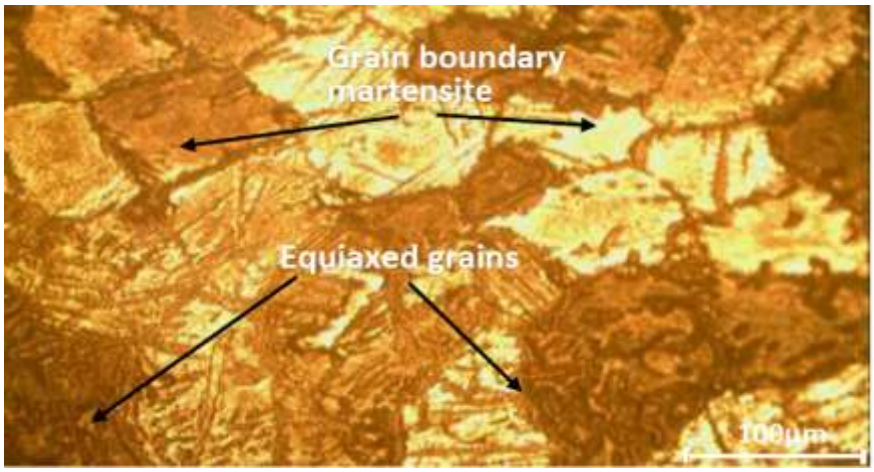


Plate 4.4: Micrograph of TIG welded ferritic stainless steel at 116J/mm (Run 16), etched with 50% Acetic-Nital (x100)

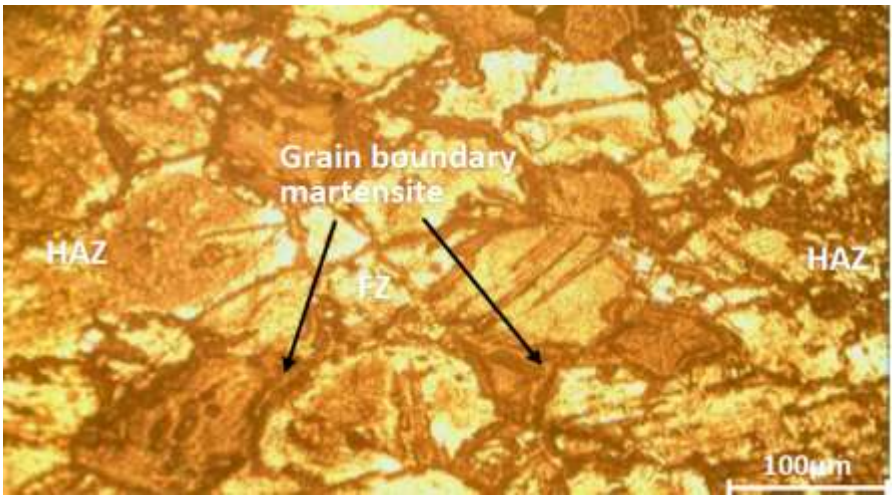


Plate 4.5: Micrograph of TIG welded ferritic stainless steel at 116J/mm (Run 18), etched with 50% Acetic-Nital (x100)

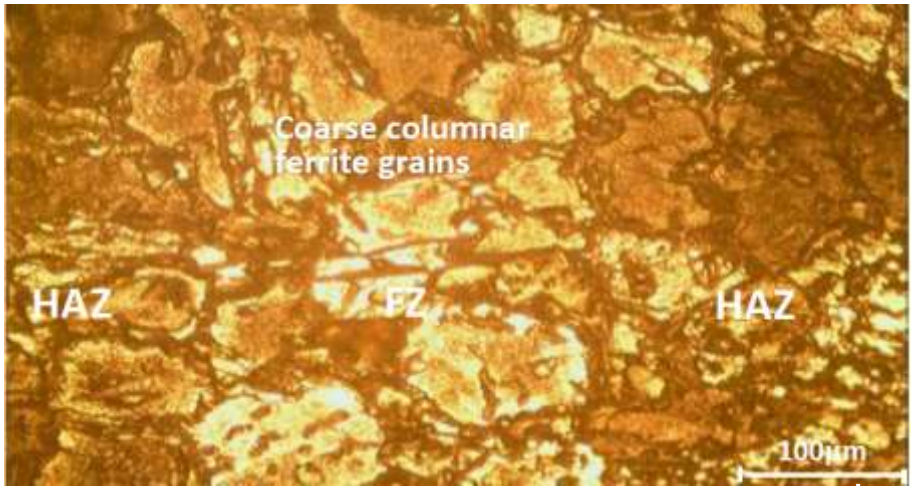


Plate 4.6: Micrograph of TIG welded ferritic stainless steel at 174J/mm (Run 14), etched with 50% Acetic-Nital (x100)

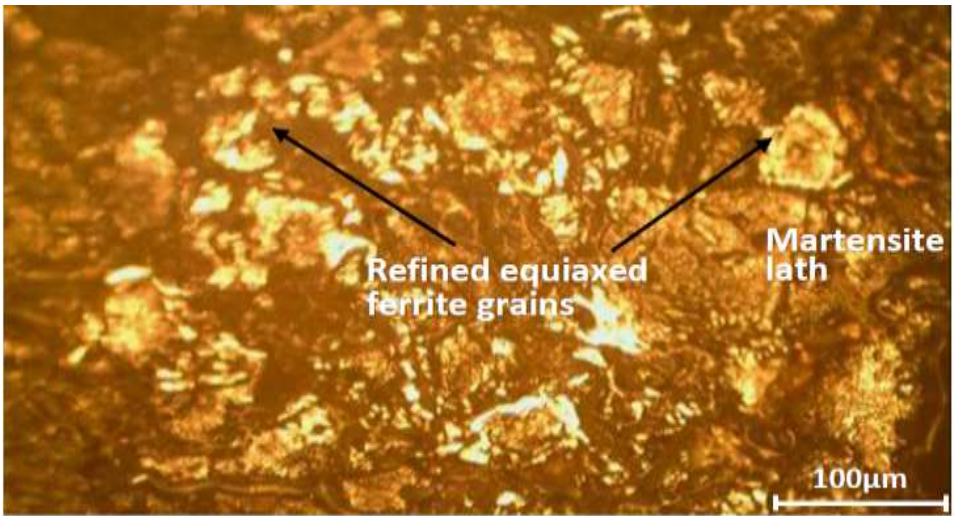


Plate 4.7: Micrograph of TIG welded ferritic stainless steel at optimized welding conditions (102J/mm), etched with 50% Acetic-Nital (x100)

Plate 4.2 shows the micrograph of the base metal (as-received) having a fine-grained ferrite microstructure aligned in the cold rolling direction. Plate 4.3 shows the micrograph of the weld with 58J/mm heat input, showing incomplete weld penetration with the presence of some primary δ ferrite as indicated by the black portions within the matrix of the structure. This is due to low heat input into the weld joint leading to some micro porosities in the structure of the weldment. Plate 4.4 and 4.5 show the micrographs of the sample welded at 116J/mm. the microstructures contains predominantly both equiaxed and columnar ferrite grain structure. As indicated in the Plates, some martensite could also be

found along the grain boundary of the welded samples. The formation of these grain boundary martensite is expected considering the amount of carbon content of 0.12% in this grade (AISI430 FSS) which widen the austenite gamma loop at elevated temperature. This austenite transforms to the grain boundary martensite at lower temperature which leads to the increase in tensile strength and hardness value as shown in experimental run 18 and 16 respectively of Table 4.1. The increase in these properties may also be attributed to increase in the formation of equiaxed ferrite grains within the microstructure of the weldments. Plate 4.6 shows the micrograph of the welded sample with 174J/mm heat input, it can be observed that as the heat energy input increases, the cooling rate is lower, allowing longer time for the grains to grow. The elevated temperature delta ferrite transforms to lower temperature ferrite which are predominantly columnar grain structures. These lower temperature ferrite phases are indicated by the white portions in the fusion and heat affected zones as shown in (Plate 4.6). The presence of these excess columnar ferrite structures as well as increase in the grain size due to high heat input lower the mechanical properties of the weld metal. Plate 4.7 shows the micrograph of the weld produced at the optimum heat input conditions which contains fine equiaxed ferrite grain structures. Some lath martensite structures could also be found to exist along the ferrite grain boundaries as a continuous grain boundary phase across the weldment as indicated in the Plate. The martensite lath was formed as a result of the transformation of the little austenite that formed at elevated temperature which suppresses the growing of ferrite grain by shortening the time spent at the grain coarsening temperature, hence, facilitated the formation of equiaxed and refined grain morphology within the fusion and heat affected zones of the welded structure (Amuda and Mridha 2011).

4.4.3 Analysis of the micro-hardness

The distribution of the hardness across the weldment measured at 1.5mm intervals is presented in Figure 4.17. The hardness was measured in the longitudinal direction under different welding conditions. The weld specimen considered were grouped into four which include, the base metal, welds with least hardness value, weld with highest hardness value and weld with the optimized conditions. From the hardness profile, it is observed that all the specimens considered followed the same trend. The fusion zone exhibits the highest hardness value and decreases gradually through the heat affected zone to the unaffected base metal.

Similar result has been reported by Budduet *al*. (2014)and Kumar *et al*. (2017). The increase in the hardness value at the fusion zone is due to formation of fine equiaxed grain and intergranular martensite on solidification (Razaullahet *al*., 2016). Experimental run 16 gives the highest hardness based on single optimization. It was also observed from Figure 4.17 that welding with heat input of 58J/mm (experimental run 9), the hardness value is lower, this could be attributed to the incomplete penetration of the welds, leading to lower properties. Similar trend was also observed in the tensile strength of the welds.

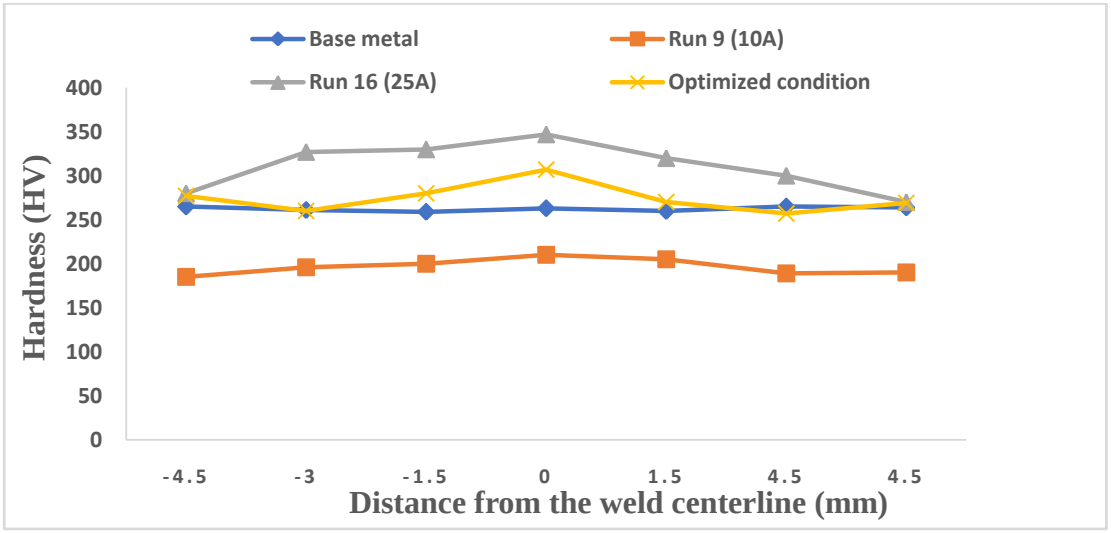


Figure 4.17: Longitudinal hardness profile across the weld section under different weld conditions

Figure 4.18 shows the influence of welding currents on the hardness of the TIG ferritic stainless steel weld, keeping other parameters at optimized values. This was obtained using the developed model equation for the hardness (Equation 4.4), and it is observed that the hardness is lower below and above the optimum value. This shows that the effect of current exhibits a parabolic trend on the hardness with its maximum value at 22A as shown in Figure 4.18. The decrease in the hardness value at higher current is due to high energy input which induces coarse grains into the weld joint. Also, current below the optimum value decreases the hardness value, this may be due to improper weld penetration, thereby creating porosities and undercut in the weldment with poor mechanical properties. Similar trend was also observed in Figure 4.19 where the hardness value was maximum at 5mm/s welding speed and decrease below and above the optimum value.

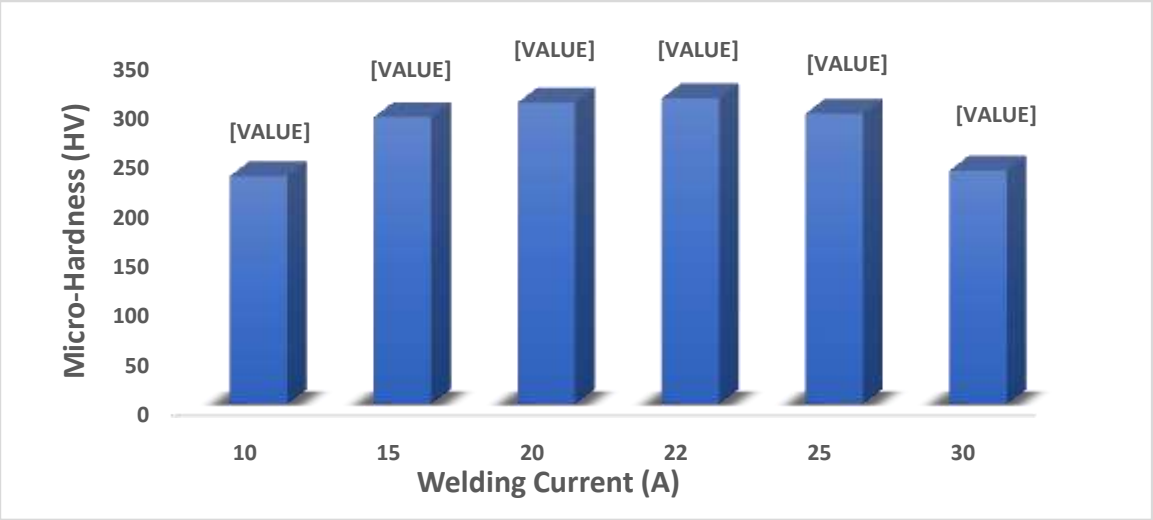


Figure 4.18: Influence of welding current on the micro-hardness of the weld.

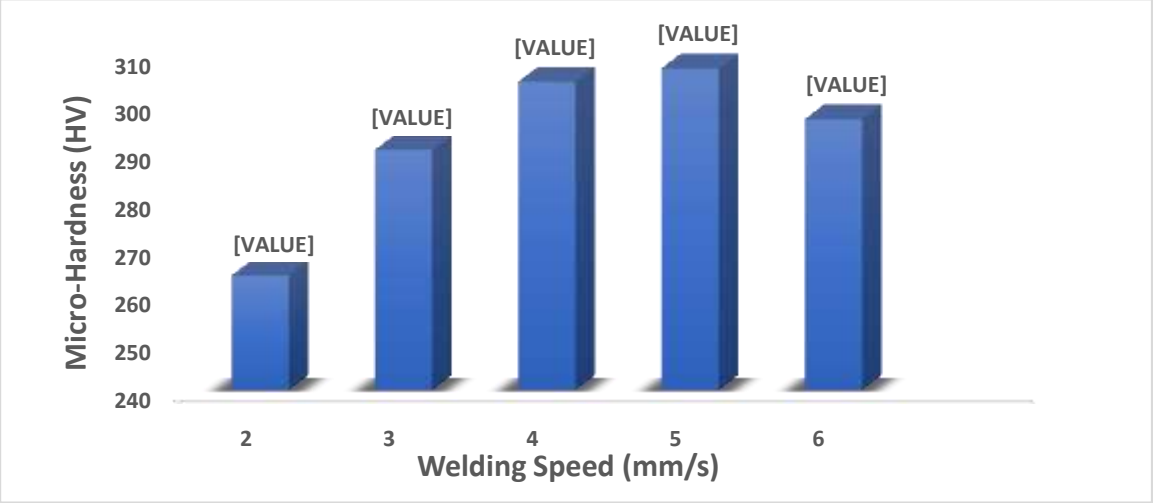


Figure 4.19: Influence of welding speed on the micro-hardness of the weld

4.4.4 Analysis of the tensile strength

Figure 4.20 shows the influence of welding current on the tensile strength of the TIG ferritic stainless steel weld while keeping the other parameters at the optimized values. It was observed from the Figure that the effect of current also exhibits a parabolic behavior on the tensile strength with its maximum value at 22A as shown in Figure 4.20. It was also observed that the strength was maximum at the optimized welding speed of 5mm/s (Figure 4.21) and decrease below and above the optimum value.

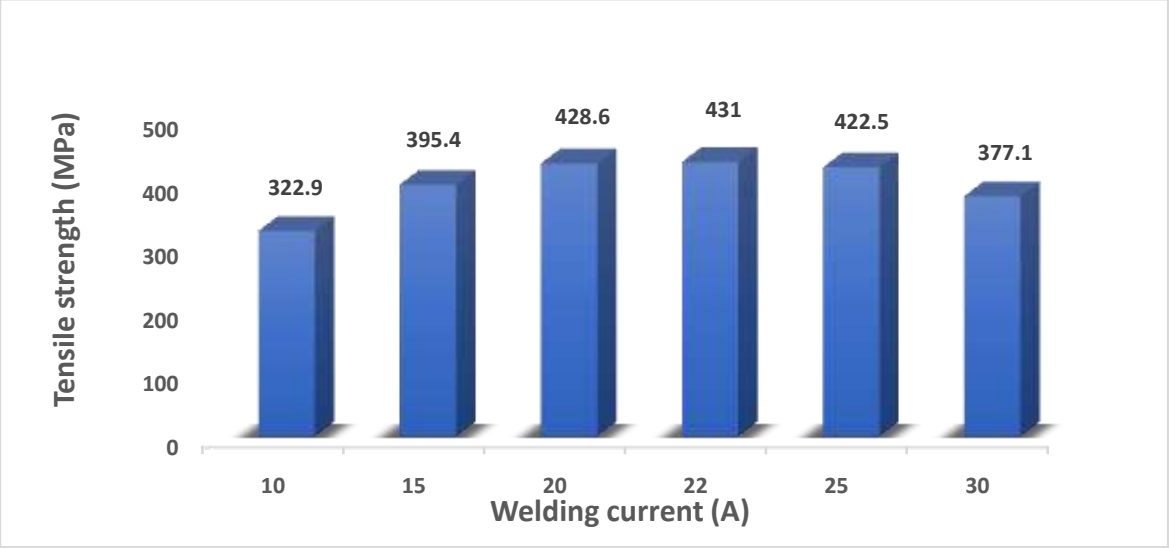


Figure 4.20: Influence of welding current on the tensile strength of the weld

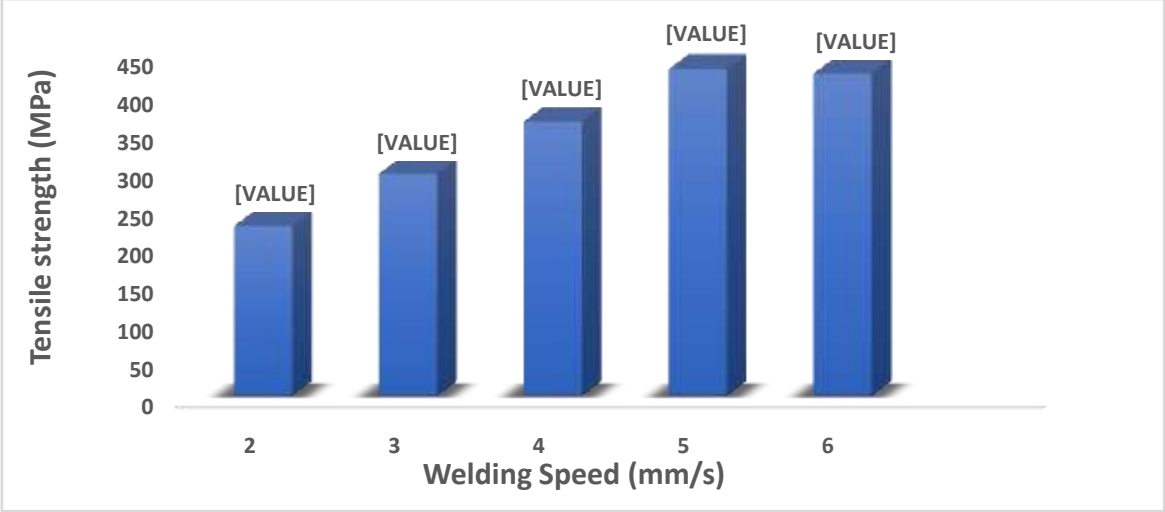


Figure 4.21: Influence of welding speed on the tensile strength of the weld

4.5 Summary

This chapter basically presents the experimental results and discussions of the parametric effect of TIG welding of ferritic stainless steel through the response surface methodology, based on central composite design (CCD). The results obtained were analyzed using design expert version 10.0 and model equations were developed for the respective responses. Figures 4.18 to 4.21 confirmed that the model equations were adequate and can be adopted to describe the behaviors of the responses considered. The multi-objective optimization process generated a set of input process parameters that give the optimum levels for the responses. The optimal solution shown in Table 4.9 indicates that all the three process parameters considered influence the outcome of the responses. Hence, the optimal values for the three parameters were set at 22A, 5mm/s and 10L/min for current, speed and argon flow rate respectively. The optimal values obtained for the tensile strength and hardness are 431.014MPa and 307.10HV respectively.

Furthermore, the influence of the process parameters was examined on the characteristic behaviors of the responses. The analysis was performed and evaluated on the responses through optical microscopy (OPM). In order to validate the results, confirmation experiment was conducted using the optimized process parameters and after the analysis of

the tests, it was observed that both the predicted and the observed response results were in a good agreement with a combined desirability of almost 1. Moreover, the percentage error for each response was 1.23% for the tensile strength and 1.81% for the hardness as presented in Table 4.10. Since the percentage errors for the two responses are within the accepted ranges of 10% as obtained in some literature studies (Kumar and Dhiman, 2013; Vidyarthy et al. 2017), therefore it can be concluded that the validity of the optimum conditions for the multiple responses is adequate and confirmed.

CHAPTER FIVE

CONCLUSION AND RECOMMENDATIONS

5.1 Conclusion

In the present study, optimization of TIG process parameters on the welding properties of AISI 430 ferritic stainless steel was investigated with the aim of controlling the heat energy input and improve the mechanical properties (tensile strength and hardness) of FSS welds. Based on the results obtained, the following conclusions were drawn from the present work;

1. Welding of TIG ferritic stainless steel at different welding parameters level using central composite experimental design was successfully achieved with improved weld quality at the optimized condition compared to welds at the two extreme heat inputs.

2. The surface topography of the optimized weld is continuous, smooth and defect free comparedto weldsatthetwoextremeheatinputs. The microstructural examination of the FSS weld reveals the presence of refined equiaxed ferrite grain structure and some martensite laths in the fusion and heat affected zones of the optimized welds which justifies the reason for the increase in the weld properties at the optimized condition.

3. The multi-objective optimal solution for the FSS weld was attained at an optimized condition of 22A (welding current), 5mm/s (welding speed) and 10L/min (argon flow rate). The resultant optimum output of 431.014MPa and 307.10HV for the tensile strength and hardness respectively, obtained at this optimized condition indicate that the weld property is close to that of the base metal.

4. The validation of the optimization process for the FSS welds showed average percentage errors of 1.23% for tensile strength and 1.81% for hardness with a combined desirability of almost 1, indicating that the weld has close properties with that of the base metal with improved hardness of 14.6% more than the base metal and a tensile strength of 3.5% less than the base metal

5.2 Recommendations

1. Based on the findings and conclusions derived in this study, it is recommended that welding of ferritic stainless steels with TIG welding parameters set at 22 A welding current, 5 mm/s welding speed and 10L/min argon flow rate produced a weld joint with improved properties that are closer to that of the base material.

2. Further research can be conducted on the same material by considering other welding parameters such as arc gap, welding voltage and electrode tip diameter to evaluates the level of improvement in the tensile and hardness property of the welds.

3. Research can also be conducted using helium as the shielding gas to evaluate and compares it shielding potential and its effects on the weld quality of TIG ferritic stainless steel welds.

5.3 Contribution to Knowledge

The current study provides opportunity to widen the scope of understanding on the use of TIG parameters selection through the optimization of the process parameters to achieve the aim of minimizing the problem of grain growth in ferritic stainless steel welds with improvement in the properties of the weldment. The following are the specific contributions of this research study to the body of knowledge.

1. The study developed empirical equations to predict the likely values of the properties (tensile strength and hardness) at any combinations of the three parameters.
2. The study established the optimal TIG welding parameters (22A current, 5mm/s speed and 10L/min argon flow rate) to achieved the optimum responses of 431.014 MPa tensile strength and 307.10 HV hardness.

References

Adebisi A.A. (2016). Optimization of stir casting process parameters of Aluminium Silicon Carbide Particulate composites. PhD thesis, pp. 145.

Ahmed, K.H., Abdul, L., Mohd, J. and Pramesh,T. (2010). Influence of welding speed on tensile strength of welded joint in TIG welding process. *Intl. Journal of Applied Engineering Research,* 1(3), pp.518-527.

American Iron and Steel Institute, 1133 15th Street, NW, Washington, DC 20005, U.S.A., in co-operation with ASM International, 2015.

Amuda, M. O. H., and Mridha, S. (2009). "Microstructural features of AISI 430 ferritic stainless steel (FSS) weld produced under varying process parameters." *Intl. J. of Mech. and Mats. Engineering* 4(2), pp.160-166.

Amuda, M.O.H and Mridha S. (2010). Grain refinement in ferritic stainless steel welds: the journey so far. *Advanced Materials Research Vols. 83-86 (2010) pp. 1165-1172.*

Amuda, M.O.H., Akinlabi, E.T. and Mridha, S. (2016). Ferritic Stainless Steels: Metallurgy, Application and Weldability. Elsevier Inc. pp. 1-17.

Amuda, M.O.H., and Mridha, S. (2011). Effect of Energy Input on Microstructure and Hardness of TIG Welded AISI 430 Ferritic Stainless Steel. *Advanced Materials Research*, pp. 390-396.

Amuda, M.O.H., and Mridha, S. (2012). Comparative evaluation of grain refinement in AISI 430 FSS by elemental powder addition and cryogenic cooling. Materials and Design, 35, pp. 609-618.

Anbazhagan V, Nagalakshmi R. (2002). Metallurgical studies in ferritic stainless steel welds. WRI J; 23(3), pp. 25–37.

Balasubramanian, V., Shanmugan, K. and Lakshminarayanam, A. K. (2008) "Effect of autogenous arc welding processes on fatigue crack growth behavior of ferritic stainless steel joints," *Iron and Steel Institute of Japan International*, vol. 48, no. 4, pp. 489–495.

Bello K.A., Maleque, M.A, Idriss A.N.M, Mirdha S. (2013). Processing of TiC-CNT hybrid composite coating on low alloy steel using TIG torch technique *Appl. Mech. Mater.* 378**:** pp. 259- 64.

Bello KA, Maleque, M.A, Ahmad Z, Mirdha, S. (2015). Optimization of Hardness Behaviour of TIG Modified Ceramic Coating Using the Taguchi Approach. *Advanced Materials Research*, pp. 238-242.

Bensaid, N. Tala-Ighil, N. Badji, R. Hadji, M. (2012). Optimization of TIG welding parameters in ferritic stainless steel (AISI 430). *ConférenceInternationale sur*. Pp. 66-73.

Bob Capudean (2003). Metallurgy Matters: Carbon content, steel classifications, alloys and steels. Oakland Community College, Auburn Hills

Bolarinwa, J.K., Saliu, O.S., Godwin I.E., Ayotunde, I.I. (2018). Review of GTAW Welding Parameters. Journal of Minerals and Materials Characterization and Engineering, (6), pp. 541-554

Box, G.E. and Behnken, D.W. (1960). Some new three levels design the study of quantitative variables. *Technometrics*, 2(4), pp. 55-75.

Buddu, R. K., Chauhan, N. and Raole, P.M. (2014). Mechanical properties and microstructural investigations of TIG welded 40 mm and 60 mm thick SS 316L samples for fusion reactor vacuum vessel applications. *Fusion Engineering and Design*12(89), 3149 – 3158.

Castro, R., and De Cadenet, J. J. (1974). *Welding Metallurgy of Stainless and Heat Resisting Steels*, Cambridge University Press, London.

Cibi, A. J, and Thilagham, K T (2017). High Frequency Gas Tungsten Arc Welding Process for Dressing of Weldment. *International Journal of Advanced Engineering Research and Science (IJAERS)*, 4(3), pp. 229-235.

Dauda E.T, Hassan S.B, Aponbiede O., Nyior G.B, Mohammed R.A. (2010). The assessment of Microstructure and hardness characteristics of some welded low carbon steels. *Nigerian Journal of engineering* 17: pp. 67-73.

Diler, E.A. and Ipek, R. (2012). An experimental and statistical study of interaction effects of matrix particle size, reinforcement particle size and volume fraction on the flexural strength of Al-SCp composite by P/M using central composite design. *Materials Science and Engineering.* 548, pp. 43-55.

Fisher, R.A (1992). The arrangement of field experiments *Breakthroughs in statistics*: 82-91, Springer

Fisher,G. J., and Maciag, R. J. (1977) in *Handbook of Stainless Steels*, Eds. McGraw-Hill, New York.

Ganesh, K.C., Vasudevan, M., Balasubramanian, K.R., Chandrasekhar, N., and Vasantharaja, P. (2014). Thermomechanical analysis of TIG welding of AISI 316LN stainless steel. *Materials Manufacturing Process,* 29, pp. 903-909

Ghasemi, R., Beidokhti, B., Fazel-Najafabadi, M. (2018). Effect of delta ferrite on the mechanical properties of dissimilar ferritic-austenitic stainless steel welds. *Arch. Metall. Mater*. 63(1), 437-443.

Higgins, R.A. (2004). Engineering Metallurgy. Viva books, New Delhi.

John, L. (2014). Design and analysis of experiment with R. New York: CRC Press. Taylor and Francis USA.

Jurica, M., Kožuh Z., Garašić, I. and Bušić, M. (2018). Optimization of the A-TIG welding for stainless steels. IOP Conference. Series: Materials Science and Engineering 329.

Katundi, D., Tosun-Bayraktar, A., Bayraktar, E., Toueix, D. (2010). Corrosion behaviour of the welded steel sheets used in automotive industry. *J. Achiev. Mater. Manuf. Eng.* 38, pp. 146–153.

Khanna, O.P. (2010). Materials Science and Metallurgy. Taj Press, New Delhi.

Kobe Steel, Ltd. (2015), "The Arc Welding of Specific Steels and Cast Irons,"

Kou, S. (2003). *Welding Metallurgy*, Wiley Inter-science, 2nd Edition.

Kumar, N., Mukherjee, M. and Bandyopadhyay, A. (2017). Study on laser welding of austenitic stainless steel by varying incident angle of pulsed laser beam. *Optics and Laser Technology* **(**94), 296 – 309.

Kumar, R. and Dhiman, S. (2013). A study of sliding wear behaviors of Al-7075 alloy and Al-7075 hybrid composite by response surface methodology analysis. *Materials and Design*, 50, 351-359.

Lakshman S., Davinder S., and Pragat S. (2013). A review: Weldability of Stainless steels. *Journal of Mechanical and Civil Engineering*. Vol. 6 pp. 24-31.

Lakshminarayanan, A.K., Shanmugam, K., Balasubramanian, V. (2009). Effect of welding processes on tensile, impact, hardness and microstructure of joints made of AISI 409M FSS base metal and AISI 308L ASS filler metals. *Ironmaking and Steelmaking.* 36, pp. 75–80.

Lokesh, K.G., Karthikeyan, P., Narasimma, R.C., Prasanna, B. and George, O. (2015) Microstructure and Mechanical Properties of ASS (304)-FSS (430) Dissimilar Joints in IN SMAW and GTAW Process. *International Journal of Engineering Sciences and Research Technology*, 6, pp. 367-378.

Mallaiah, G., Kumar, A., Ravinder, P.R. and Madhusudhan, G. R. (2012). Influence of grain refining elements on mechanical properties of AISI 430 ferritic stainless steel weldments -Taguchi approach.*Materials and Design,* 36, pp. 443–450

Mallaiah, G., Ravinder, P.R., Kumar, A. (2014). Influence of titanium addition on mechanical properties, residual stresses and corrosion behaviour of AISI 430 grade ferritic stainless steel GTA welds. Procedia Materials Science, 6, pp. 1740 – 1751.

Marcell Gáspár (2019). Effect of Welding Heat Input on Simulated HAZ Areas in S960QL High Strength Steel. *Institute of Materials Science and Technology, University of Miskolc.* Pp. 1 – 14

Mike Sammons (2007). Welding austenitic stainless steel. 2741 N. Roemer Road Appleton, WI 54911

Mohandas T, Reddy GM and Naveed M. (1999). A comparative evaluation of gas tungsten and shielded metal arc welds of a ferritic stainless steel. *J Mater Process Technol*, 94, pp. 133–40.

Mridha, S. and Amuda, M. O. H., (2011). An Overview of Sensitization Dynamics in Ferritic Stainless SteelWelds.*International Journal of Corrosion*, pp 1-9.

Myers, R. H., Montgomery, D. C. and Anderson-Cook, C. M. (2009). Response Surface Methodology: Process and Product Optimization Using Design Experiment (3rd ed.). New Jersey: John Wiley and Sons. Inc.

Navaneeswar, G.R. and Venkata, M.R. (2018). Optimization of process parameters in welding of dissimilar steels using robot TIG welding. *IOP Conf. Series: Materials Science and Engineering*330, pp. 1-7.

Parmer, R. A (2010). Welding Engineering and Technology. Khanna Publishers, New Delhi.

Pekkarinen, J. and Kujanpää, V. (2010). The effects of laser welding parameters on the microstructure of ferritic and duplex stainless steels weld. *Phys. Proc. 5, Part A*, 517–523.

Penuela, L.E., Smart B. and peter J. (2009). Analysis of dissimilar welds exposed to high temperature conditions. *Journal of science and technology.*

Rajput ER. R. K. (2013). Material science and engineering, 4th ed. S.K Kataria& Sons.

Ramkumar, K.D, Aditya, C., Aditya K.S., Sharang A., Anurag, A., Arivazhagan, N. and Arul M.R. (2015). Comparative studies on the weldability, microstructure and tensile properties of autogeneous TIG welded AISI 430 ferritic stainless steel with and without flux. *Journal of Manufacturing Processes,* 20, 54-69.

Ravinder, S. K. and Jarial. (2015). Parametric Optimization of TIG Welding on Stainless Steel (202) and Mild Steel by using Taguchi Method. *International Journal of Enhanced Research in Science Technology & Engineering*, 4 (6), 484-494.

Razaullah K. M., Pathak, A. K., Umasankar, D. and Dhirendra, T. (2016). Study of Microstructure and Mechanical Properties of Feritic Stainless Steel (AISI 430) Weldment using ER309L and ER430 electrodes by MIG welding process. *International Journal of Engineering Research & Technology*, 5(1), pp. 312-318.

Richard, E. (2012). Guidelines for welding dissimilar steels. *Journal of sci. and engineering*, 1(1), pp.27-36.

Roger Andersson (2005). Deformation Characteristics of Stainless Steels. PhD Thesis, Luleå University of Technology Department of Applied Physics and Mechanical Engineering

Sabioni, A., Claret, S., Anne, M.H, Elizete, C.L, Marc, M., and Christian, H. (2003). Comparative study of high temperature oxidation behaviour in AISI 304 and AISI 439 stainless steels. *MaterialsResearch* 6(2), pp. 179-185.

Sanjay, K., Pravin, K.S., Dharmendra, P. and Prasad, S.B. (2017). Optimization of TIG welding process parameters using taguchi's analysis and response surface methodology. *International Journal of Mechanical Engineering and Technology*, 8(11), pp. 932–941.

Sanjay, K.G., Avinash, R.R., Meghanshu, V., MohdZaheer, K.Y. (2018). Effect of heat input on microstructure and mechanical properties in gas metal arc welding of ferritic stainless steel. *Materials Research Express*, pp. 1-17.

Santos, B., Farias, C., Sobral, M., Moises A., Oliveira, and Matheus S.S ARAUJO. (2012). "Spectral analysis of ultrasonic lamb waves applied to the study of the intermetallic phase presence on plates of AISI 430 ferritic stainless steel submitted to isothermal treatments." In *18th World Conf. on Nondestructive Testing*, pp. 1-10.

Sathiya, P., Aravinda, S., NoorulHaq, A. (2007). Effect of friction welding parameters on mechanical and metallurgical properties of ferritic stainless steel. *International Journal of Advanced Manufacturing Technology*, 31, pp. 1076–82.

Sharmistha, S. and Neha, G. (2016). Analysis of Hardness in Metal Inert Gas Welding of Two Dissimilar Metals, Mild Steel & Stainless Steel. *IOSR Journal of Mechanical and Civil Engineering (IOSR-JMCE)*, 13(3), pp. 94-113.

Subhas, C. M., Pradip, K.P. and Asish, B. (2019). Design Optimization of TIG Welding Process for AISI 316L Stainless Steel. *Intl. Journal of Recent Technology and Engineering (IJRTE)*, 8(2), pp. 5348-5354.

Subhas, C. M., Pradip, K.P., Asish, B. and Rudrapati, R. (2018). Determination of tungsten inert gas welding input parameters to attain maximum tensile strength of 316l austenitic stainless steel. *Journal of Mechanical Engineering*, 68(3), pp. 231 – 248.

Ugla, A.A. (2018). Enhancement of weld quality of AISI 304L austenitic stainless steel using a direct current pulsed TIG arc. *IOP Conference Series: Materials Science and Engineering*, pp. 1-15.

Vidyarthy, R. S., Dwivedi, D. K and Vasudevan, M. (2017). Optimization of A-TIG Process Parameters Using Response Surface. *Materials and Manufacturing Processes.* pp. 1-31.

Vijayan, D., Seshagiri, V.R. (2018). Process Parameter Optimization in TIG Welding of AISI 4340 Low Alloy Steel Welds by Genetic Algorithm. IOP Conf. Series: Materials Science and Engineering (**390)** 012066 doi:10.1088/1757-899X/390/1/012066.

Villafuerte, J.C, Pardo, E. and Kerr, H.W. (1990). The effect of alloy composition and welding conditions on columnar-equiaxed transitions in ferritic stainless steel gas tungsten arc welds. *Metall Trans A*, 21, pp. 2009–2019.

APPENDIX A